NACA RM A53I23

NACA

RESEARCH MEMORANDUM

DOWNWASH BEHIND A TRIANGULAR WING OF ASPECT RATIO 3 - TRANSONIC BUMP METHOD

By John A. Axelson

Ames Aeronautical Laboratory
Moffett Field, Calif.

CLASSIFIED DOCUMENT

This material contains information affecting the National Defense of the United States within the meaning of the espionage laws, Title 18, U.S.C., Secs. 793 and 794, the transmission or revelation of which in any manner to an unauthorized person is prohibited by law.

NATIONAL ADVISORY COMMITTEE
FOR AERONAUTICS

WASHINGTON

December 1, 1953

1S

NACA RM A53I23

NATIONAL ADVISORY COMMITTEE FOR AERONAUTICS

RESEARCH MEMORANDUM

DOWNWASH BEHIND A TRIANGULAR WING OF ASPECT RATIO 3 — TRANSONIC BUMP METHOD

By John A. Axelson

SUMMARY

An investigation of the lift, drag, pitching-moment, and downwash characteristics of a triangular wing of aspect ratio 3 having an NACA 63A006 section has been conducted at Mach numbers from 0.6 to 1.1 through the use of the transonic bump of the Ames 16-foot wind tunnel. The corresponding Reynolds numbers based on the mean aerodynamic chord of the wing varied from 1.8 million to 2.4 million.

Downwash was measured by means of an all-movable horizontal tail at five locations. Expressed in wing semispans, the tail heights were 0, ±0.20, and 0.40 at a tail length of 1.33, and a tail height of 0.40 at a tail length of 1.00, the tail lengths being measured aft from the lateral axis through the quarter point of the mean aerodynamic chord of the wing. The angle-of-attack range extended beyond that for wing stall at all but the highest Mach number of 1.10.

INTRODUCTION

Wings of triangular plan form have assumed considerable importance in the design of high-speed aircraft because of their aerodynamic and structural properties. Recently a comprehensive comparison of theoretical and experimental aerodynamics of triangular wings in combination with a body has been published in reference 1 for both subsonic and supersonic speeds. Only limited information exists, however, on downwash and its related effects on horizontal tails used in conjunction with triangular wings. Methods for predicting downwash have been limited to idealized conditions and are not generally suitable for higher angles of attack at transonic and supersonic speeds, as shown in references 2 and 3.

Earlier experimental investigations of the transonic downwash of triangular wings are presented in references 4, 5, and 6. In reference 4,

an investigation of a wing having an aspect ratio of 2 and a modified NACA 0005 section is reported; while in references 5 and 6, studies of wings of aspect ratio 4 having an 8-percent-thick, modified double-wedge section and an NACA 65A006 section, respectively, are reported. A somewhat limited range of tail locations was covered in reference 4; while in references 5 and 6, the maximum angles of attack were 8° and 10°, respectively. In the present report, transonic downwash results for a triangular wing having an aspect ratio of 3 are presented over a wide range of angles of attack up to slightly beyond stall for all but the highest test Mach number of 1.10.

Many factors enter the choice of tail location. The earlier studies reported in references 4 and 5 and low-speed investigations reported in references 7, 8, 9, and 10 concluded that generally superior longitudinal stability characteristics resulted with the horizontal tail on or near the extended plane of the wing. Placing the tail above the wing plane usually resulted in adverse stability characteristics because of the regions of excessive downwash which occurred at moderate and high lifts and which, when acting on the tail, resulted in a destabilizing contribution from the tail. Consideration of additional factors, however, such as the necessary tail-to-ground clearance at the high angles of attack required for landing and take-off, the effects of landing-flap deflection, the wake of the wing and its possible influence on tail buffeting, and the necessity of keeping the tail out of the blast from jet engines has prompted many designers to choose high, forward locations, near or atop the vertical tail. Another advantage of such a placement is the possible improvement of the effectiveness of the vertical tail as discussed, for example, in reference 11. In light of the foregoing considerations, a wide range of tail positions was covered in the present investigation, including a high position involving a short tail length. The tail positions and the tail plane used for measuring the inclination of the air stream are shown in figure 1.

SYMBOLS

b wing span, ft

C_D drag coefficient, $\frac{\text{drag}}{qS}$

C_L lift coefficient, $\frac{\text{lift}}{qS}$

C_m pitching-moment coefficient referred to the quarter point of the wing mean aerodynamic chord, $\frac{\text{pitching moment}}{qS\bar{c}}$

c local wing chord, ft

[redacted]

$\bar{c}$ mean aerodynamic chord, $\frac{\int_0^{b/2} c^2 dy}{\int_0^{b/2} c\, dy}$, ft

i_t tail incidence angle, measured from wing chord plane, deg

M free-stream Mach number

M_l local Mach number

q free-stream dynamic pressure, lb/sq ft

S wing area, sq ft

y lateral distance along wing span

α angle of attack, deg

ϵ effective downwash angle, deg

$\frac{d\epsilon}{d\alpha}$ rate of change of effective downwash angle with angle of attack

APPARATUS AND TESTS

Wind Tunnel and Equipment

The model was tested on the transonic bump of the Ames 16-foot high-speed wind tunnel. A description of the bump may be found in reference 12. Lift, drag, and pitching moments were measured by means of an electrical-type strain-gage balance mounted inside the bump.

Description of the Model

A photograph of the model with the horizontal tail in position 3 is shown in figure 2; the geometric and dimensional data are presented in table I and figure 1. The tail had the same plan form as that used in the earlier investigation reported in reference 4, but the thickness-to-chord ratio was increased to 5.46 percent. There was a gap of approximately 1/16 inch between the tail and the plate. All components of the model were made of steel.

[redacted]

Evaluation of Mach Number

Typical contours of the Mach numbers measured over the bump with no model present are shown in figure 3, where the outline of the model has been superimposed to indicate its relative position. Mach number gradients existed over the model, becoming more pronounced at the highest speeds, but no attempt has been made to evaluate their effects. The free-stream Mach numbers shown in the results are the averages existing over the wing of the model. The free-stream dynamic pressures corresponded to these free-stream Mach numbers. The Mach number range extended from 0.60 through 1.10, with a corresponding Reynolds number range from 1.8 million to 2.4 million, based on the mean aerodynamic chord of the wing.

Precision

The precisions of the measurements presented in this report have been established from considerations of repeatability of data for identical conditions, sensitivity of the measuring and recording instruments, and other sources of error such as the downward stream inclination which prevailed over the bump. The Mach numbers are accurate within ±0.01; the lift coefficients are accurate to ±0.005; while the drag and pitching-moment coefficients are accurate to ±0.001. The model angle of attack with respect to the bump and the tail incidence was set within ±0.1°, but a downflow of the air stream prevailed over the bump and varied slightly with Mach number. A uniform correction of -0.6° has been applied to the angle of attack in the lift curves for the basic wing shown in figure 4, and a corresponding drag correction of $-0.010\ C_L$ has been applied to the drag polars in figure 5. The downwash angles were determined from the variations of pitching-moment coefficient with angle of attack and, subject to their corresponding precisions, were accurate within ±0.3°. The parameter $d\epsilon/d\alpha$ was evaluated within ±0.08.

Procedure

The lift, drag, and pitching-moment characteristics of the wing were determined as part of a systematic wing-plan-form investigation being conducted in the Ames 16-foot wind tunnel. To obtain the characteristics of the wing alone, the wing was tested in the position indicated in figure 3, and a plate smaller than that shown in figures 1 through 3 was used at the root of the wing. In addition to the previously mentioned corrections for stream inclination, the drag tare of the small plate has been subtracted from the results for the wing alone.

[redacted]

The effective downwash was evaluated by applying the relation $\epsilon = \alpha + i_t$ to the intersection points of the tail-on and tail-off pitching-moment curves, these points representing conditions where the pitching-moment contribution of the tail was zero. Since the plate shown in figures 1 and 2 was attached for both the tail-on and tail-off pitching-moment measurements used in evaluating downwash, no plate tare corrections have been applied, because the intersection points, of primary interest here, would be unchanged.

RESULTS AND DISCUSSION

Basic Wing Characteristics

The lift, drag, and pitching-moment characteristics for the basic wing, presented in figures 4, 5, and 6, respectively, show that at angles of attack above 8°, reductions occurred in the lift-curve slope at all Mach numbers and in the static longitudinal stability at all subsonic Mach numbers. At supersonic Mach numbers, the reduction in static longitudinal stability occurred at a higher angle of attack, around 18°. In addition, at lower lift coefficients the static longitudinal stability increased with increasing Mach number. Such characteristics, while presenting problems of aerodynamic-center travel, are common to most triangular wings. The same general trends were reported in references 1 and 13, which present evidence that the decrease in static longitudinal stability above 8° at subsonic Mach numbers does not occur for wings having aspect ratios of the order of 2 or less. In reference 13, the tips were removed from a triangular wing of aspect ratio 3 which had exhibited the decreased subsonic stability at high angles of attack. The aerodynamic characteristics of the resulting trapezoidal wing of aspect ratio 2 differed little from those of a triangular wing of equal aspect ratio, neither of which exhibited the decreased stability. As indicated in figure 4, maximum lift was obtained during the present investigation at an angle of attack of about 24° at all test Mach numbers except 1.10.

Stability Contribution of the Tail

The variations of pitching-moment coefficient with angle of attack shown in figure 7 for the model with the tail in each of the four positions indicate the most favorable longitudinal stability characteristics with the tail in the plane of the wing (position 1). In each of the other three positions, the tail was destabilizing over most of the range of angles of attack between 10° and 24°. In positions 2 and 3 the destabilizing effect was greater and occurred at lower angles of attack than in position 4, the latter involving a shorter tail length and a

correspondingly smaller tail effectiveness. The variations of pitching-moment coefficient with angle of attack for several incidences of the tail in each of the four positions are shown in figures 8 through 11, the reduced spacing of the curves in the latter figure giving an indication of the reduced effectiveness of the tail in position 4. The increase in the slopes of the curves at the higher Mach numbers is largely a result of the increased static longitudinal stability of the wing as was mentioned in reference to figure 5. Although triangular wings are often used with no horizontal tail, the addition of a horizontal tail, while a possible source of drag, generally improves the landing and take-off performance as discussed in reference 7. The tail also provides damping of the short-period longitudinal oscillation which may become critical at transonic speeds for tailless aircraft employing triangular wings of aspect ratio greater than about 2, according to evidence presented in reference 14.

Downwash

The variations of effective downwash angle with angle of attack for each of the four tail locations are summarized in figure 12, and the rates of change of downwash angle with angle of attack are shown in figure 13. The results for position 2 at negative angles of attack may be considered as representative of a fifth tail position at the same tail length but below the wing chord plane extended. Over the range of angles of attack between $\pm 8^\circ$, the downwash and $d\epsilon/d\alpha$ were greatest in position 1 and about equal in the other tail locations. At angles of attack above 10°, the smallest downwash occurred in position 5, where the tail might be expected to contribute more to the stability than in the other positions. The smaller downwash in position 5 (below the wing plane extended) might be important during landing or take-off because the decreased downwash would tend to reduce the angle of attack for tail stall of a fixed surface or to increase greatly the range required of a movable surface.

The rates of change of downwash angle with angle of attack shown in figure 13 exceeded unity for positions 2, 3, and 4 in the range of angles of attack between about 10° and 24°, which, of course, accounts for the destabilizing effect of the tail noted earlier in reference to the pitching-moment curves in figures 7 through 11. At low angles of attack, the greatest variation in $d\epsilon/d\alpha$ with increasing Mach number occurred in position 1. The effects of Mach number are believed to be primarily associated with changes in the wing-section loading characteristics.

The two distinct portions of the curves in figure 13 may be related to the two phases of loading which occur on triangular wings. Up to angles of attack of about 8°, the flow is attached over the entire span

and the section lift curves for the inner portion of the span have relatively low slopes (ref. 15) characteristic of wings of low aspect ratio. In the range of angles of attack between about 10° and those near maximum lift, stall progresses inward from the tips, the section lift curves for the inner part of the span have greatly increased slopes, and there is an almost linear reduction in the span of the trailing vortex with increasing angle of attack (fig. 15 of ref. 16). A further understanding and possibly a useful correlation of the downwash results might be possible if the corresponding section lift characteristics of the inner portion of the wing span were available, since this part of the wing had the predominating influence on the downwash at the tail locations covered in the present investigation. The development of a satisfactory analytical method for correlating or predicting downwash requires an understanding of the load distribution on triangular wings, including the effects of angle of attack, Mach number, Reynolds number, section, and aspect ratio. It is recommended, therefore, that future research on the downwash characteristics of triangular wings should, where possible, include the determination of the load distribution on the wing.

CONCLUDING REMARKS

Downwash measurements have been presented for several tail locations behind a triangular wing having an aspect ratio of 3 for Mach numbers from 0.6 to 1.1. The relationship of downwash and of tail contribution to the static longitudinal stability of the wing have been discussed.

For angles of attack below 8°, the downwash and rate of change of downwash with angle of attack were greatest in the wing plane extended (position 1). Correspondingly, the smallest tail contribution to static longitudinal stability occurred here. The variations of downwash with angle of attack were qualitatively the same at the other tail locations for angles of attack below 8°. The largest variations of downwash with increasing Mach number occurred in position 1.

At angles of attack above 10°, the rates of change of downwash with angle of attack exceeded unity at the three tail locations above the wing plane extended (positions 2, 3, and 4). The tail was, therefore, destabilizing, but the reduced tail length associated with the high, forward location (position 4) resulted in the smallest effect of the tail on the static longitudinal stability. Large reductions in the rate of change of downwash with angle of attack occurred at the lower

tail locations (positions 1 and 5) at angles of attack above 10°, with correspondingly large increases in the tail stability contributions.

Ames Aeronautical Laboratory
National Advisory Committee for Aeronautics
Moffett Field, Calif., Sept. 23, 1953

REFERENCES

1. Hall, Charles F.: Lift, Drag, and Pitching Moment of Low-Aspect-Ratio Wings at Subsonic and Supersonic Speeds. NACA RM A53A30, 1953.

2. Weil, Joseph, Campbell, George S., and Diederich, Margaret S.: An Analysis of Estimated and Experimental Transonic Downwash Characteristcs as Affected by Plan Form and Thickness for Wing and Wing-Fuselage Configurations. NACA RM L52I22, 1952.

3. Perkins, Edward W., and Canning, Thomas N.: Investigation of Downwash and Wake Characteristics at a Mach Number of 1.53. II - Triangular Wing. NACA RM A9D20, 1949.

4. Allen, Edwin C.: Investigation of a Triangular Wing in Conjunction with a Fuselage and Horizontal Tail to Determine Downwash and Longitudinal-Stability Characteristics — Transonic Bump Method. NACA RM A51F12a, 1951.

5. Walker, Harold J., and Stivers, Louis S., Jr.: Investigation of the Downwash and Wake Behind a Triangular Wing of Aspect Ratio 4 at Subsonic and Supersonic Mach Numbers. NACA RM A50I14a, 1950.

6. Sleeman, William C., Jr., and Becht, Robert E.: Aerodynamic Characteristics of a Delta Wing with Leading Edge Swept Back 45°, Aspect Ratio 4, and NACA 65A006 Airfoil Section. Transonic-Bump Method. NACA RM L9G22a, 1949.

7. Graham, David, and Koenig, David G.: Tests in the Ames 40- by 80-Foot Wind Tunnel of an Airplane Configuration With an Aspect Ratio 2 Triangular Wing and an All-Movable Horizontal Tail — Longitudinal Characteristics. NACA RM A51B21, 1951.

8. Koenig, David G.: Tests in the Ames 40- by 80-Foot Wind Tunnel of an Airplane Configuration With an Aspect Ratio 3 Triangular Wing and an All-Movable Horizontal Tail — Longitudinal and Lateral Characteristics. NACA RM A52L15, 1953.

[redacted]

9. Graham, David, and Koenig, David G.: Tests in the Ames 40- by 80-Foot Wind Tunnel of an Airplane Configuration With an Aspect Ratio 4 Triangular Wing and an All-Movable Horizontal Tail — Longitudinal Characteristics. NACA RM A51H10a, 1951.

10. Jaquet, Byron M.: Effect of Horizontal-Tail Position, Area, and Aspect Ratio on Low-Speed Static Longitudinal Stability and Control Characteristics of a 60° Triangular-Wing Model Having Various Triangular-All-Movable Horizontal Tails. NACA RM L51I06, 1951.

11. Riley, Donald R.: Effect of Horizontal-Tail Span and Vertical Location on the Aerodynamic Characteristics and an Unswept Tail Assembly in Sideslip. NACA TN 2907, 1953.

12. Axelson, John A., and Taylor, Robert A.: Preliminary Investigation of the Transonic Characteristics of an NACA Submerged Inlet. NACA RM A50C13, 1950.

13. Emerson, Horace F., and Gale, Bernard M.: Transonic Aerodynamic Characteristics of Three Thin Triangular Wings and a Trapezoidal Wing, All of Low Aspect Ratio. NACA RM A52D21, 1952.

14. Tobak, Murray: Damping in Pitch of Low-Aspect-Ratio Wings at Subsonic and Supersonic Speeds. NACA RM A52L04a, 1953.

15. Anderson, Adrien E.: Chordwise and Spanwise Loadings Measured at Low Speed on Large Triangular Wings. NACA RM A9B17, 1949.

16. Spreiter, John R., and Sacks, Alvin H.: The Rolling Up of the Trailing Vortex Sheet and Its Effect on the Downwash Behind Wings. Jour. Aero. Sci., vol. 18, no. 1, Jan. 1951, pp. 21-32, 72.

[redacted]

TABLE I.- GEOMETRIC CHARACTERISTICS OF THE MODEL

Semispan wing

Area, sq ft	0.260
Semispan, ft	0.625
Root chord, ft	0.833
Mean aerodynamic chord, ft	0.556
Aspect ratio	3.00
Taper ratio	0
Section	NACA 63A006

Horizontal tail (all-movable)

Exposed area, sq ft	0.022
Exposed semispan, ft	0.211
Root chord, ft	0.141
Tip chord, ft	0.071
Taper ratio	0.500
Aspect ratio	4.00
Hinge line, percent chord	50.0
Thickness, percent chord	5.46
Section	Modified double wedge

Tail positions (Tail heights from the wing plane and tail lengths from the quarter point of the mean aerodynamic chord of the wing, expressed in wing semispans)

Position	Height	Length
1	0	1.33
2	.20	1.33
3	.40	1.33
4	.40	1.00
[a]5	-.20	1.33

[a]Obtained by using the data for position 2 in the negative angle-of-attack range

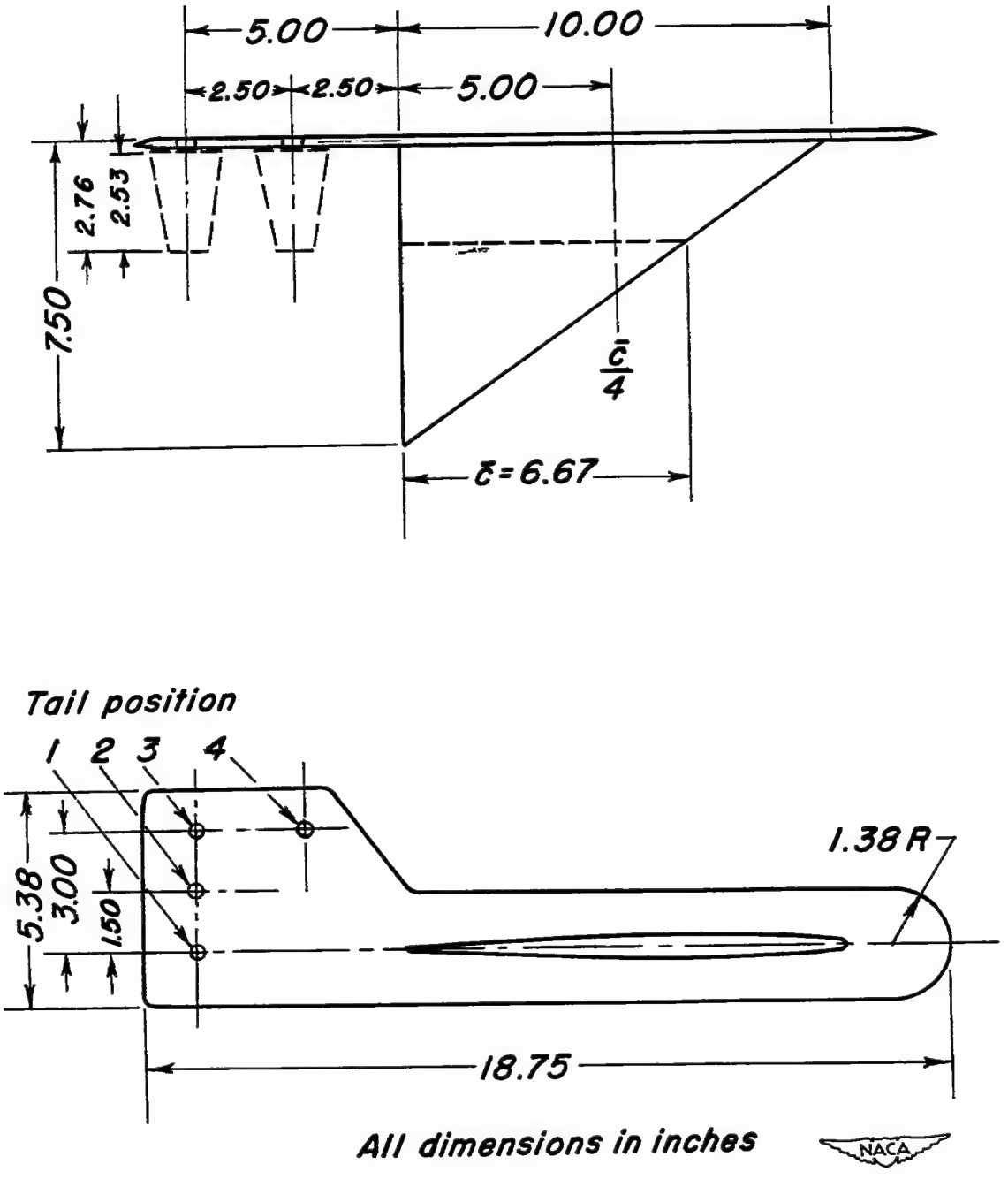

Figure 1.- Dimensional details of model.

[redacted]

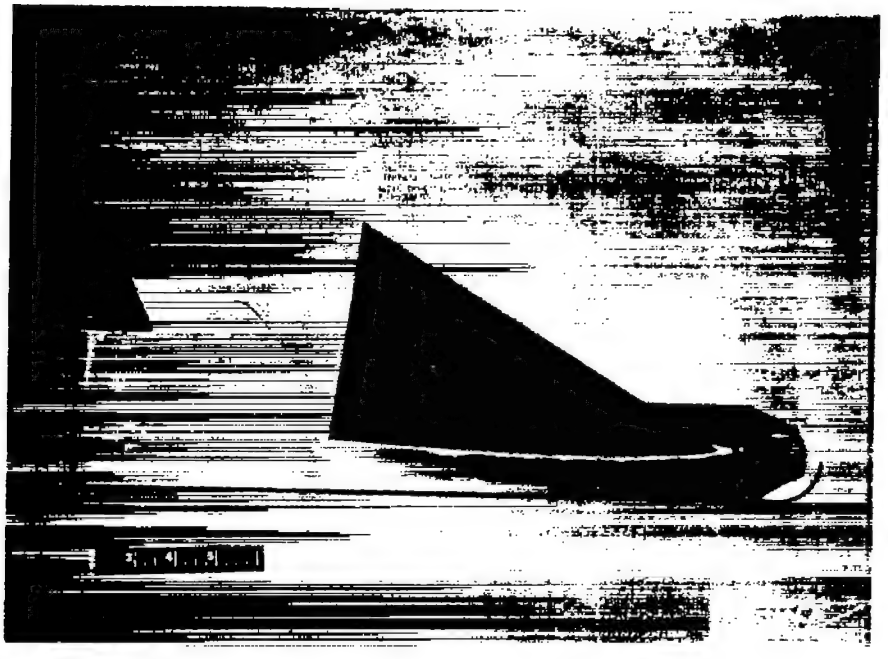

Figure 2.- Photograph of the model.

[redacted]

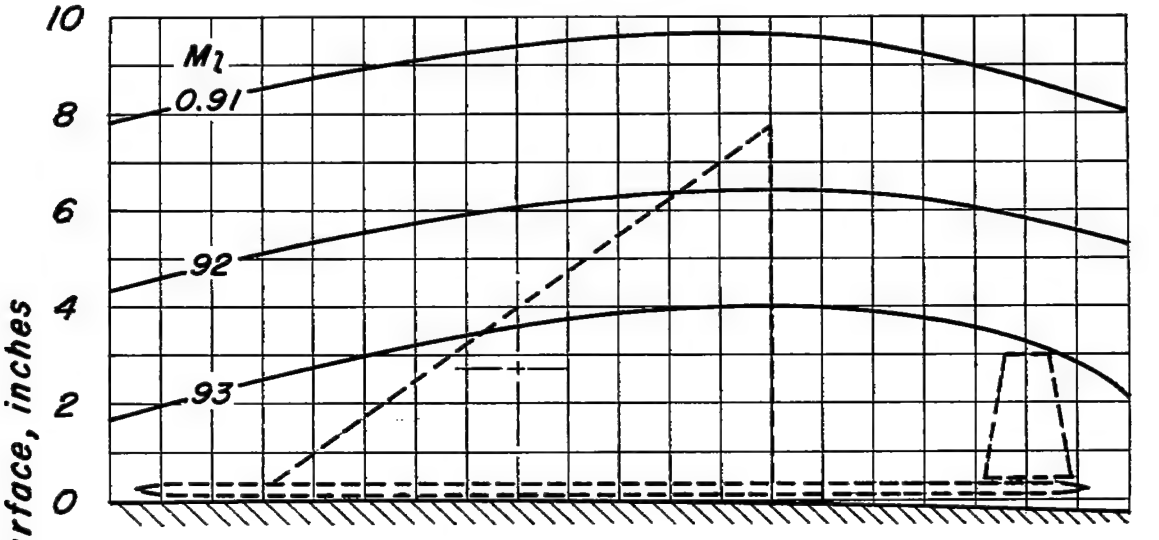

(a) M, 0.93

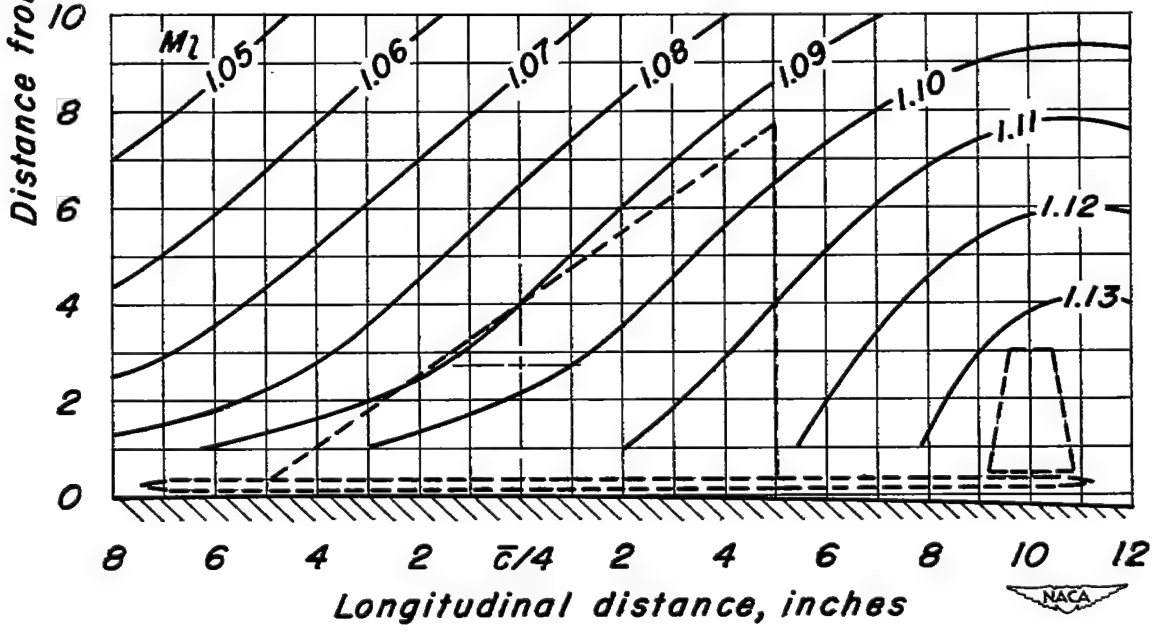

(b) M, 1.10

Figure 3.- Typical Mach number contours over the bump at the model location.

[redacted]

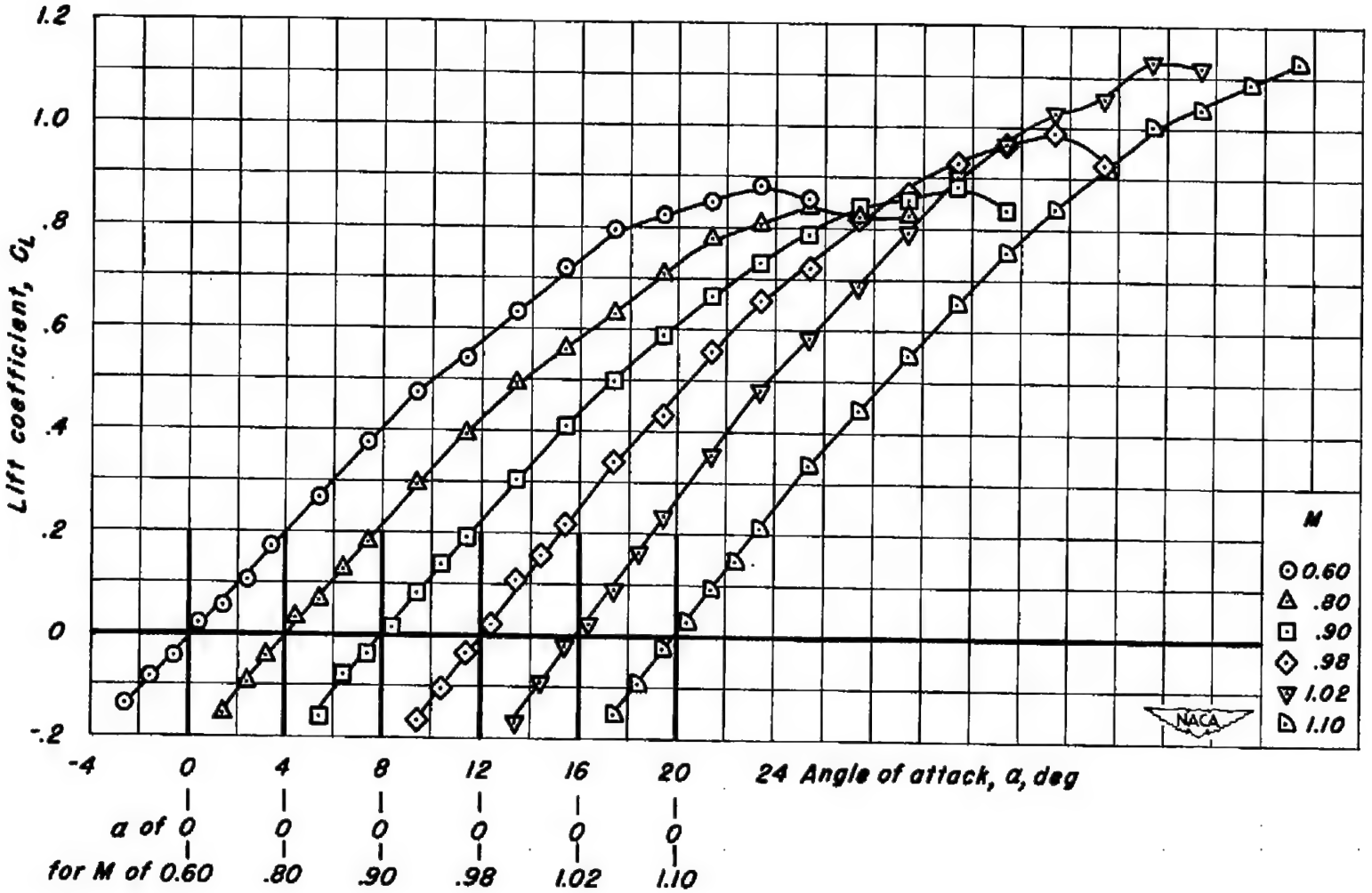

Figure 4.- Variation of lift coefficient with angle of attack at several Mach numbers for the triangular wing of aspect ratio 3.

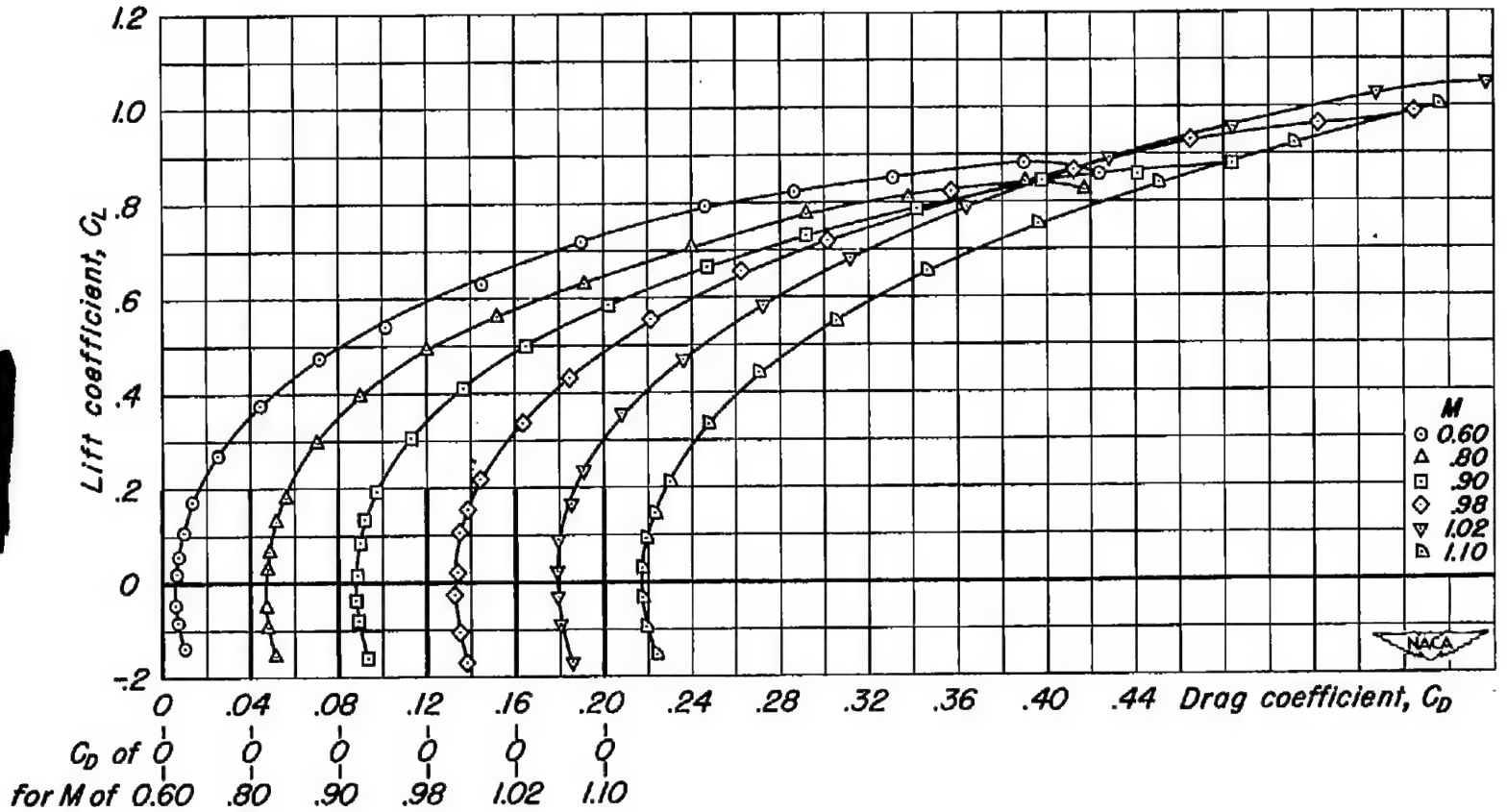

Figure 5.- Variation of drag coefficient with lift coefficient for the triangular wing of aspect ratio 3.

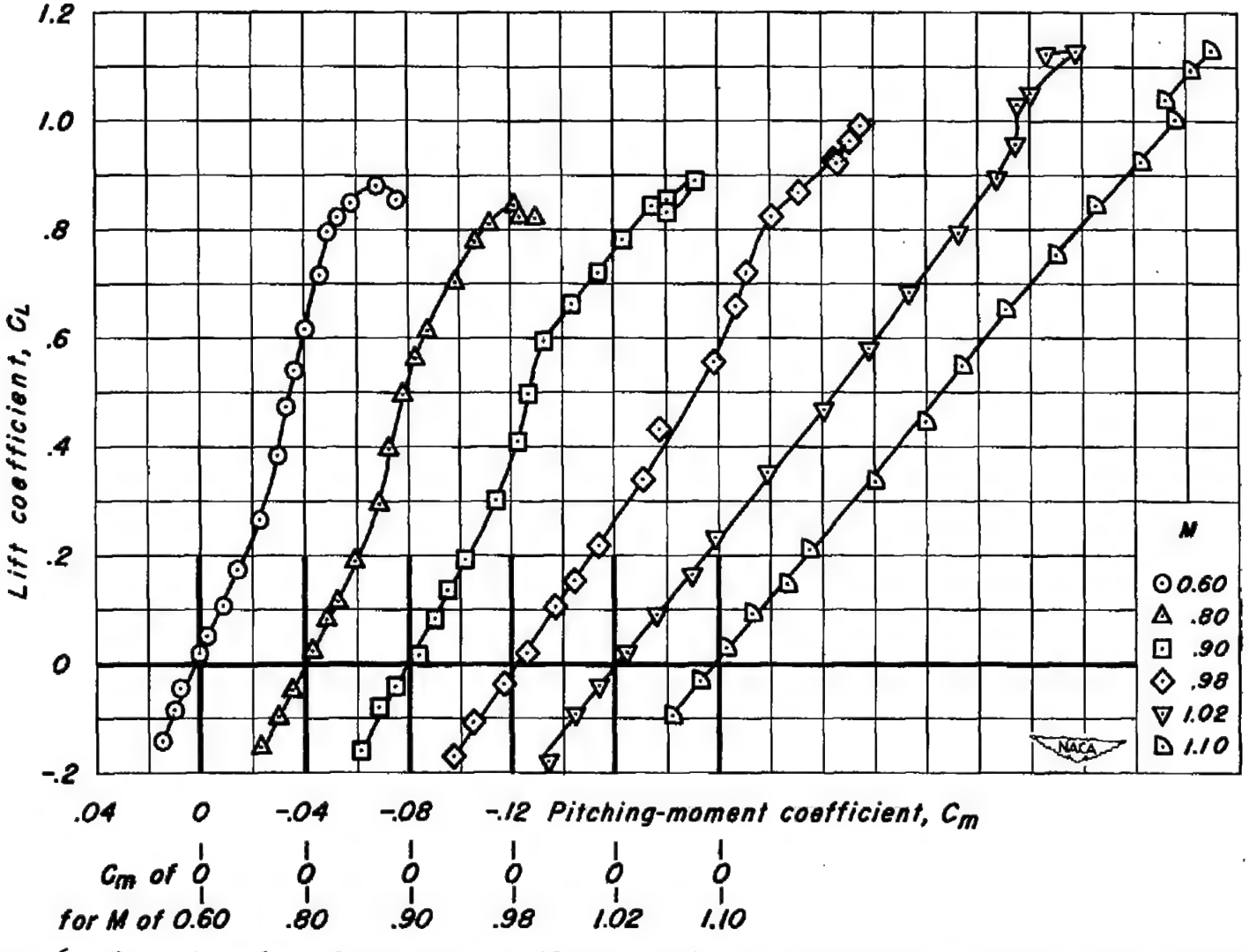

Figure 6.- Variation of pitching-moment coefficient with lift coefficient at several Mach numbers for the triangular wing of aspect ratio 3.

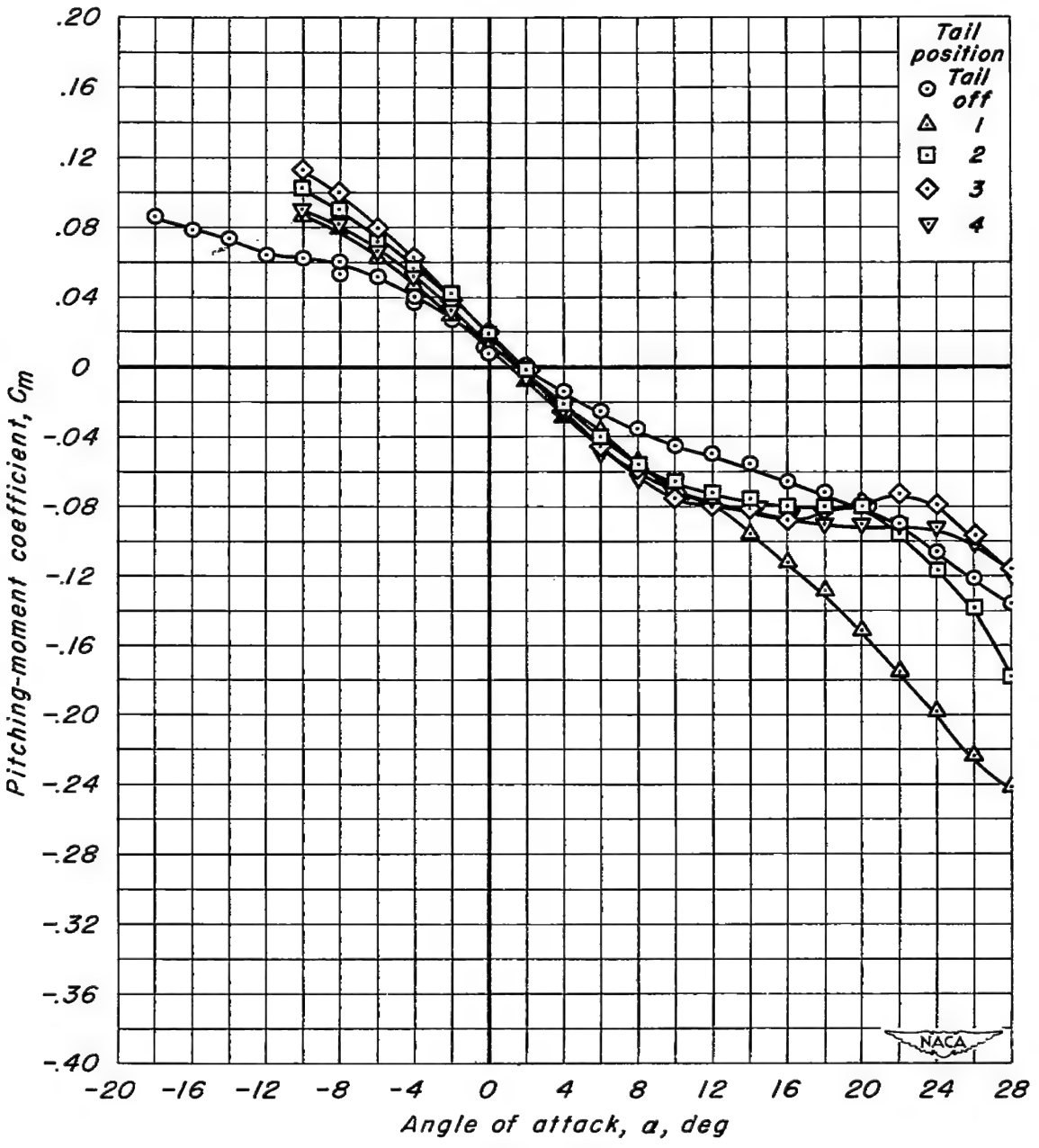

(a) M, 0.60

Figure 7.- Effects of the horizontal-tail location on the variation of pitching-moment coefficient with angle of attack. Tail incidence, 0°.

[redacted]

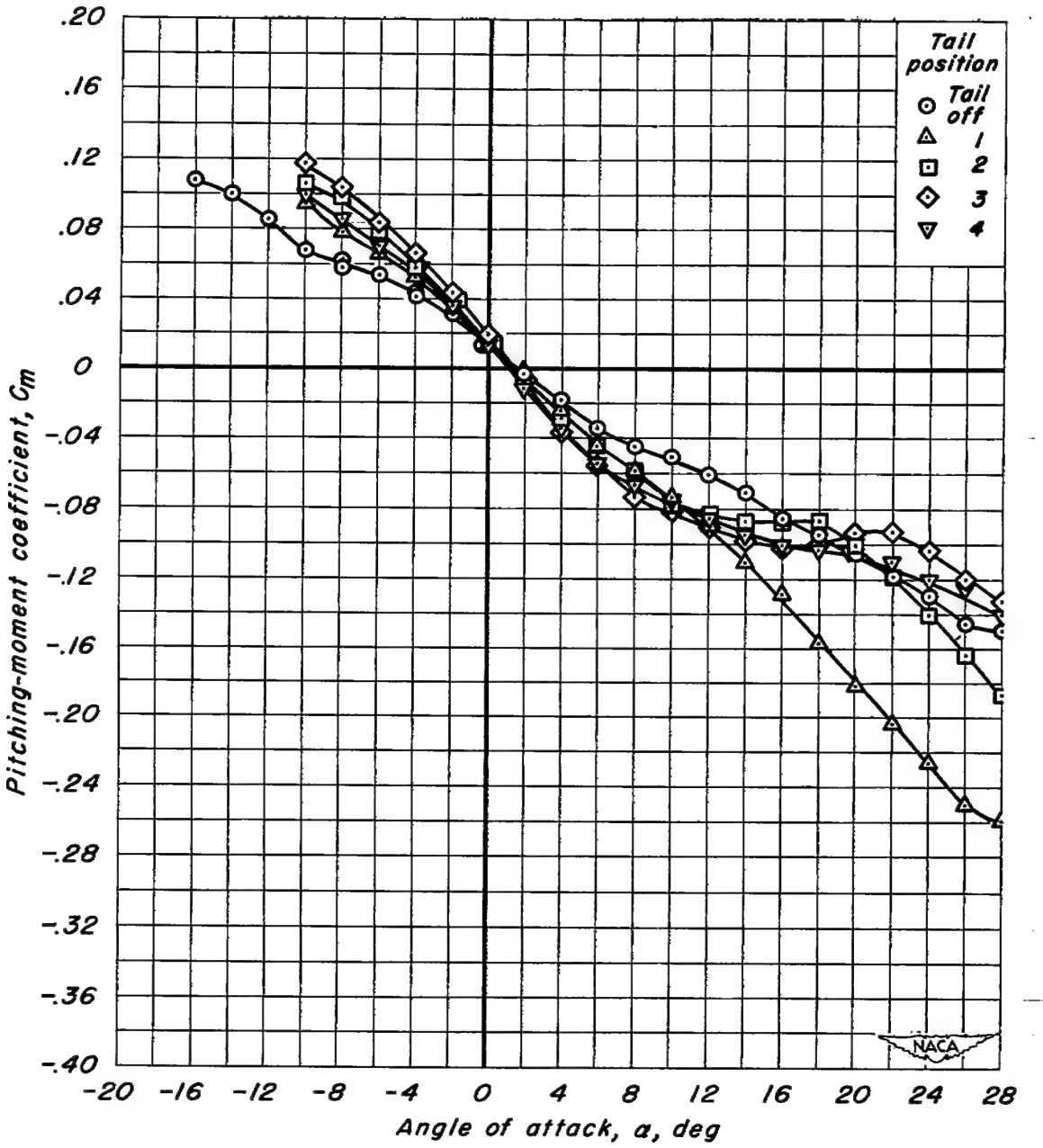

(b) M, 0.80

Figure 7.- Continued.

[redacted]

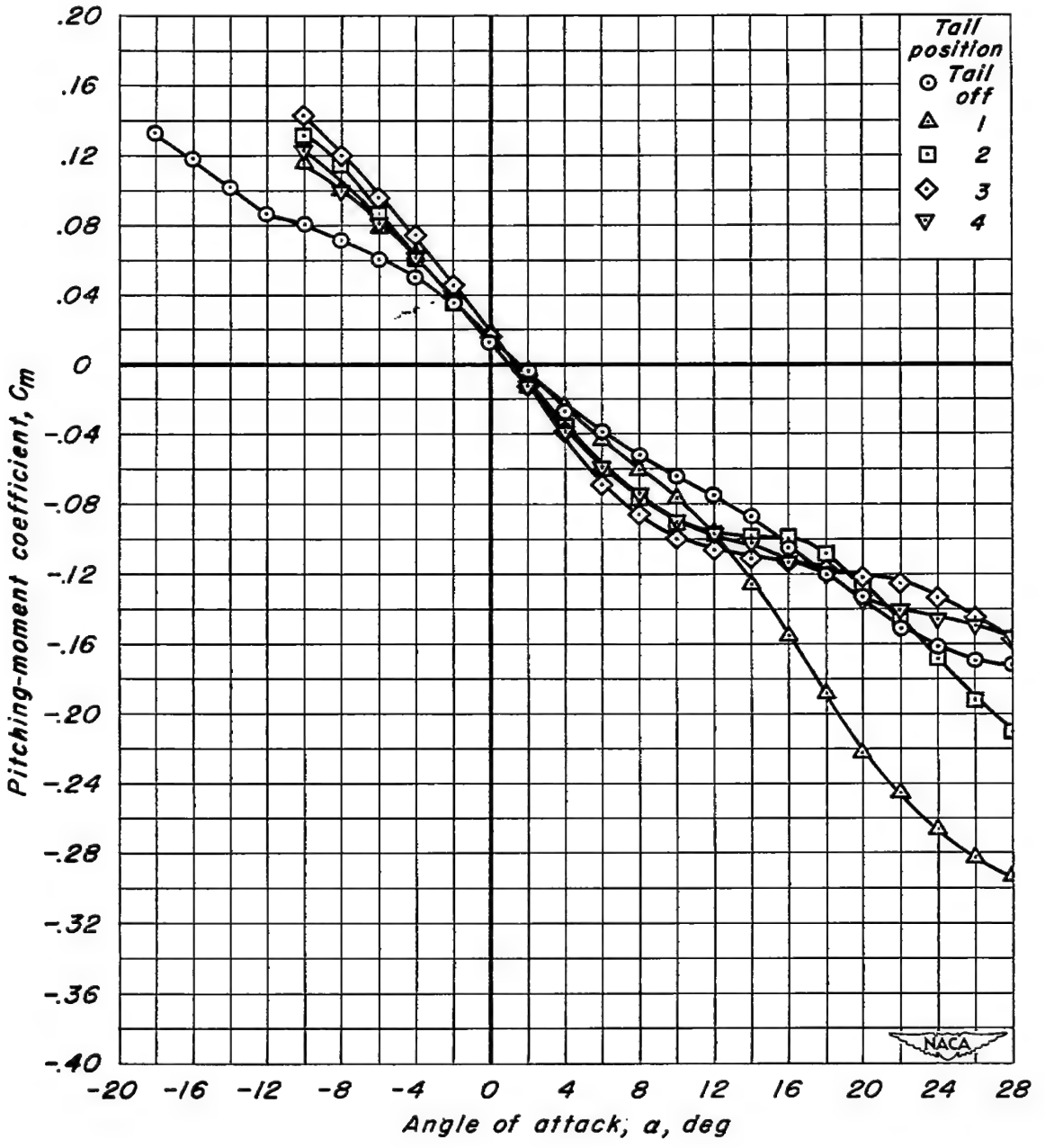

(c) M, 0.90

Figure 7.- Continued.

[redacted]

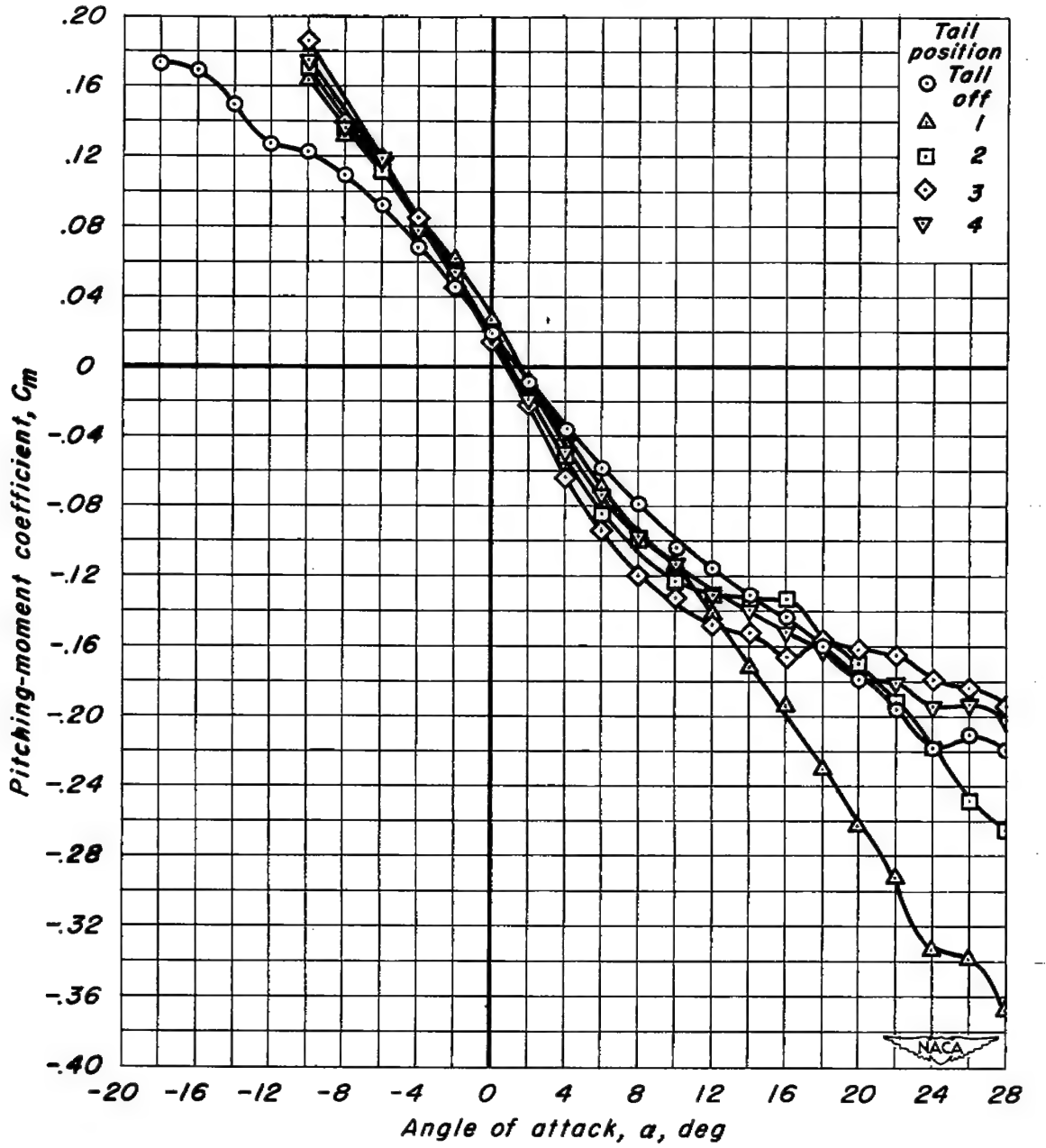

(d) M, 0.98

Figure 7.- Continued.

[redacted]

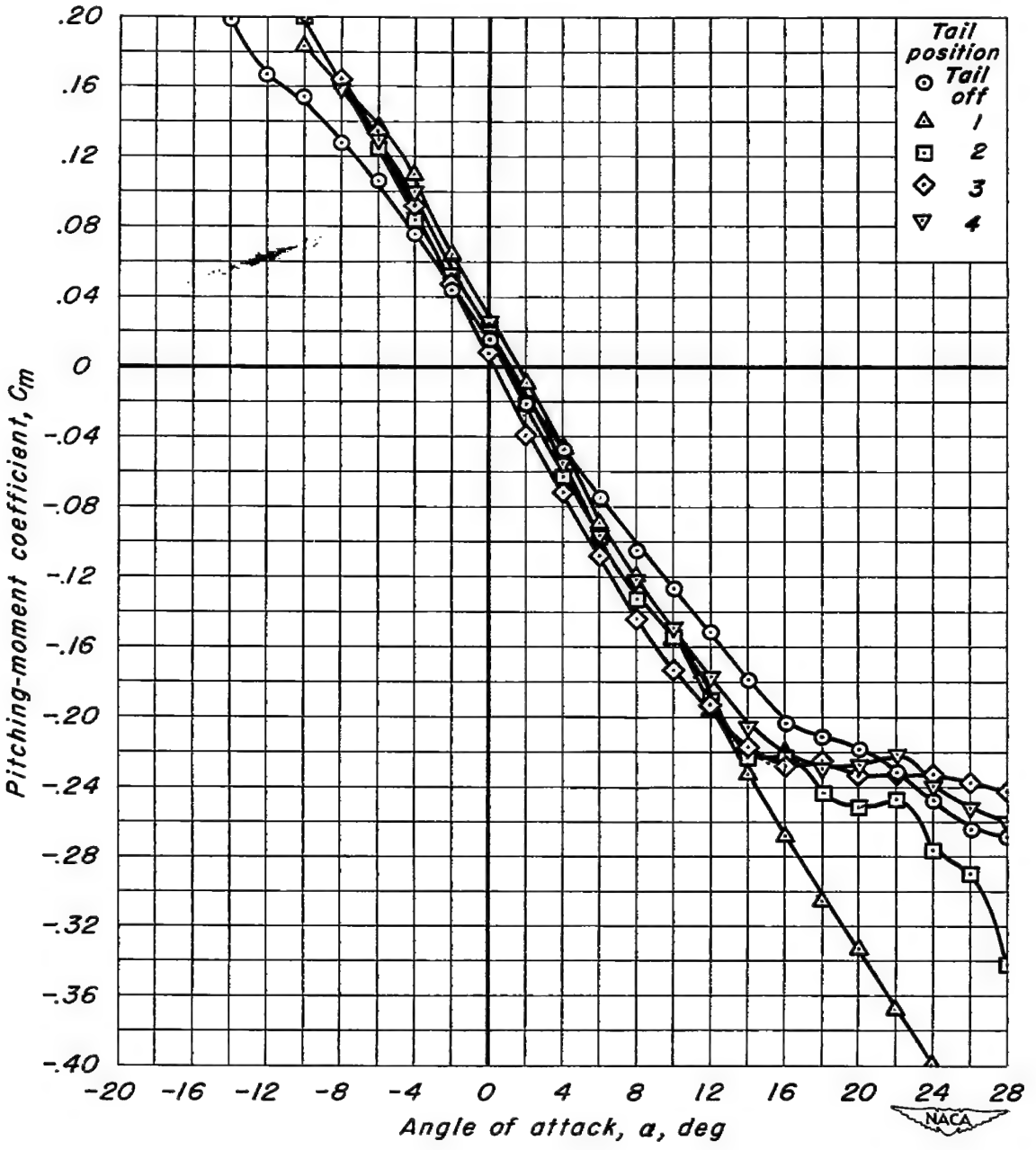

(e) M, 1.02

Figure 7.- Continued.

[redacted]

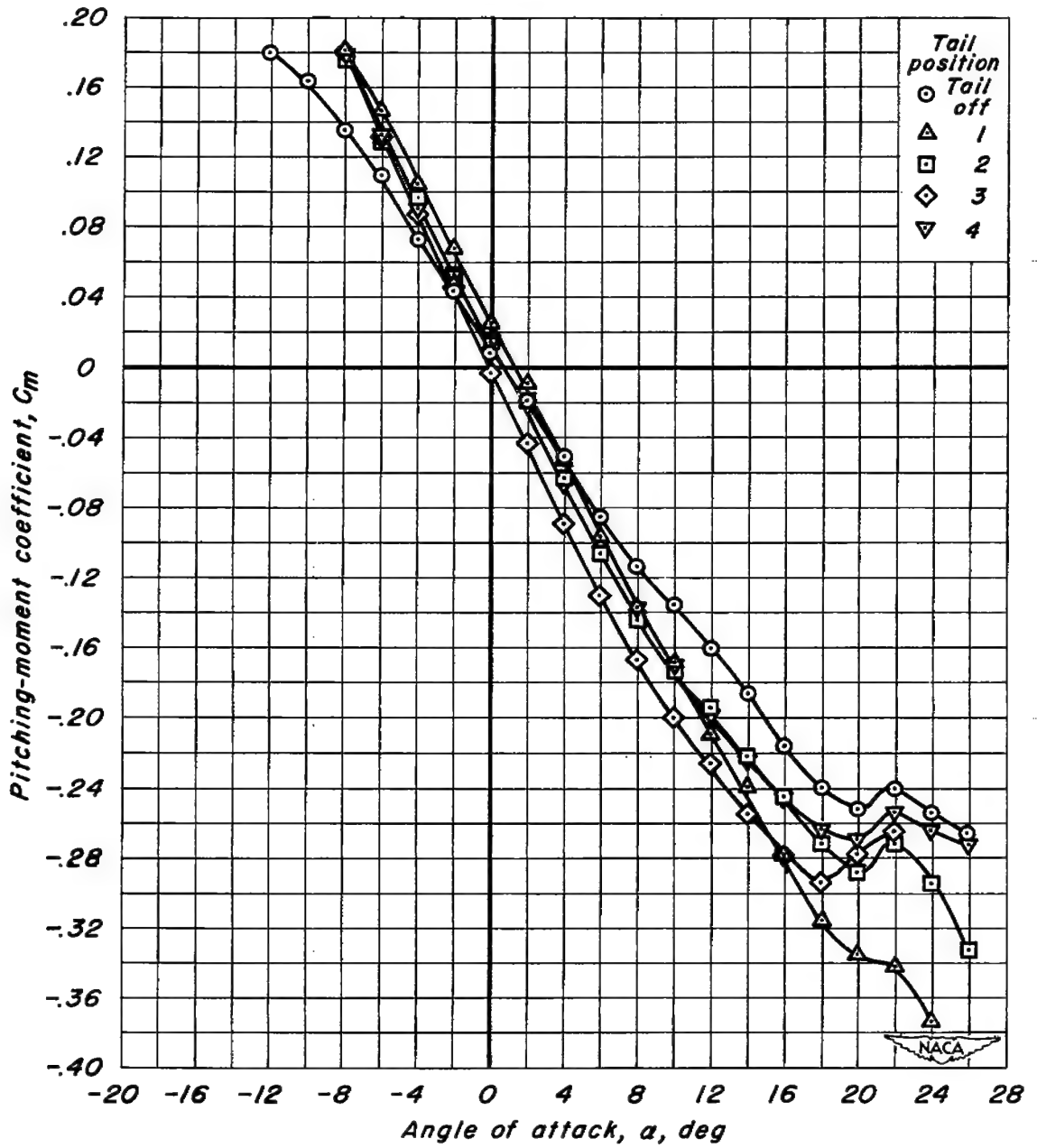

(f) M, 1.10

Figure 7.- Concluded.

[redacted]

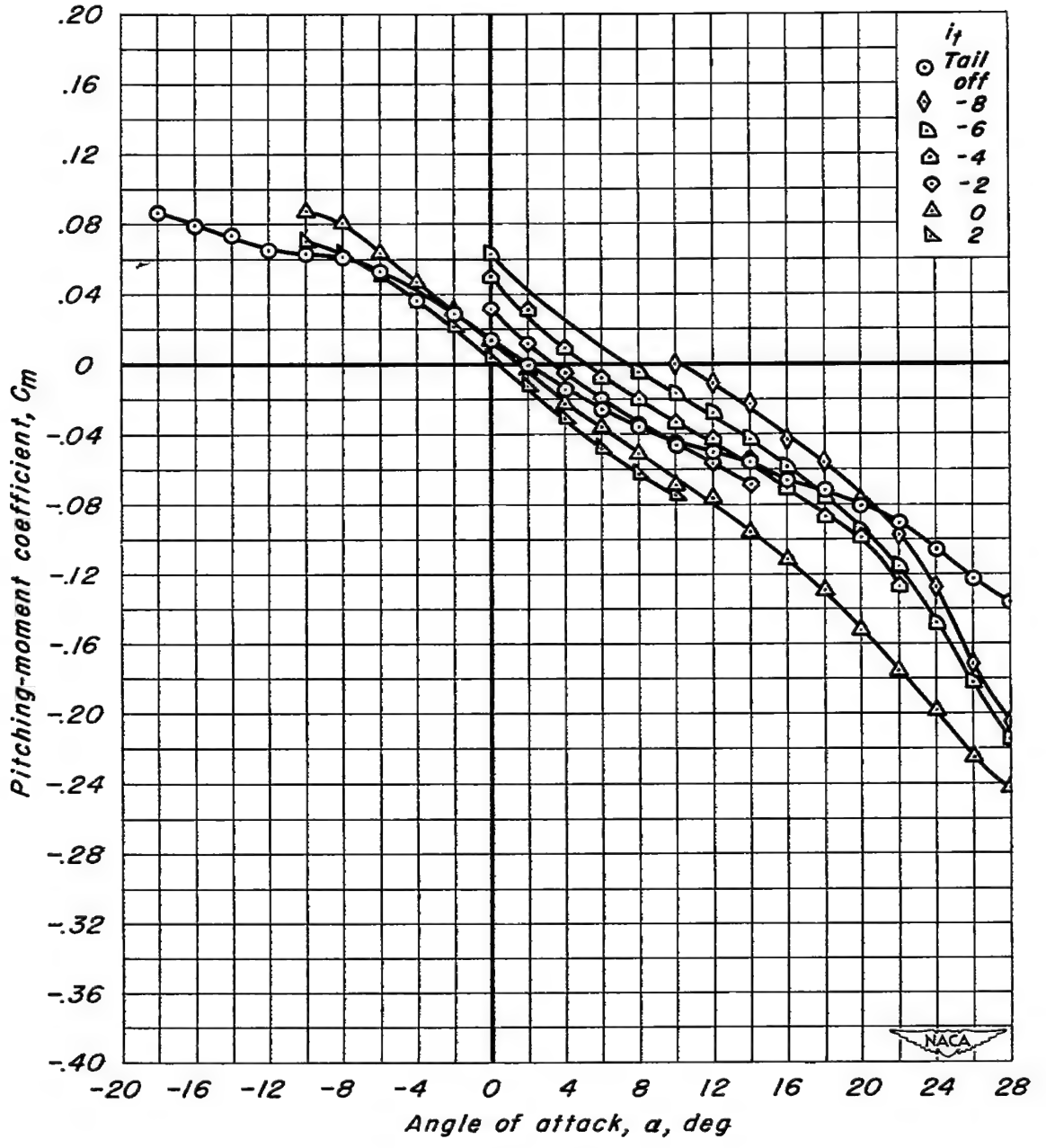

(a) M, 0.60

Figure 8.- Variation of pitching-moment coefficient with angle of attack for several incidence angles of the horizontal tail in position 1.

[redacted]

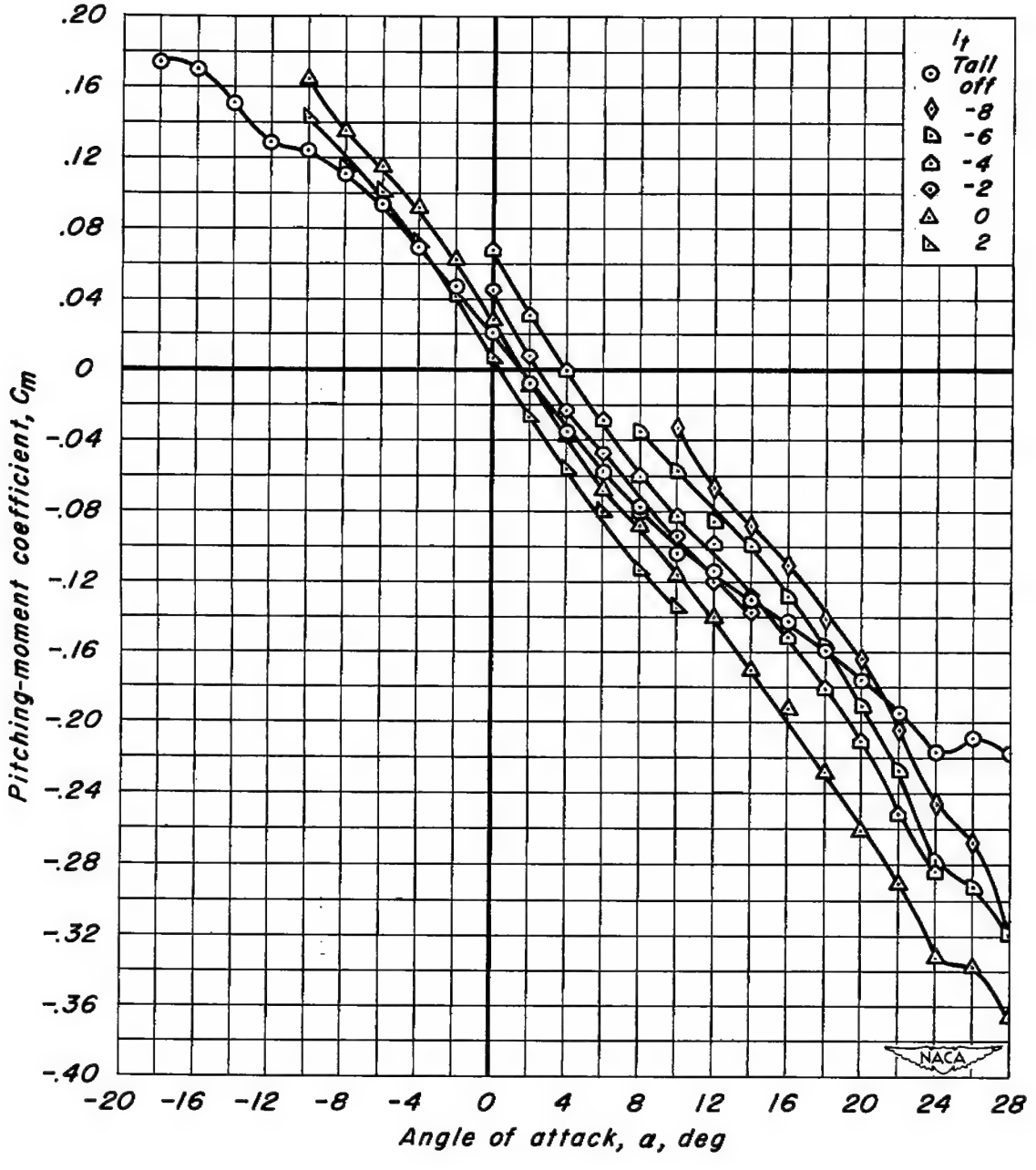

(b) M, 0.98

Figure 8.- Continued.

[redacted]

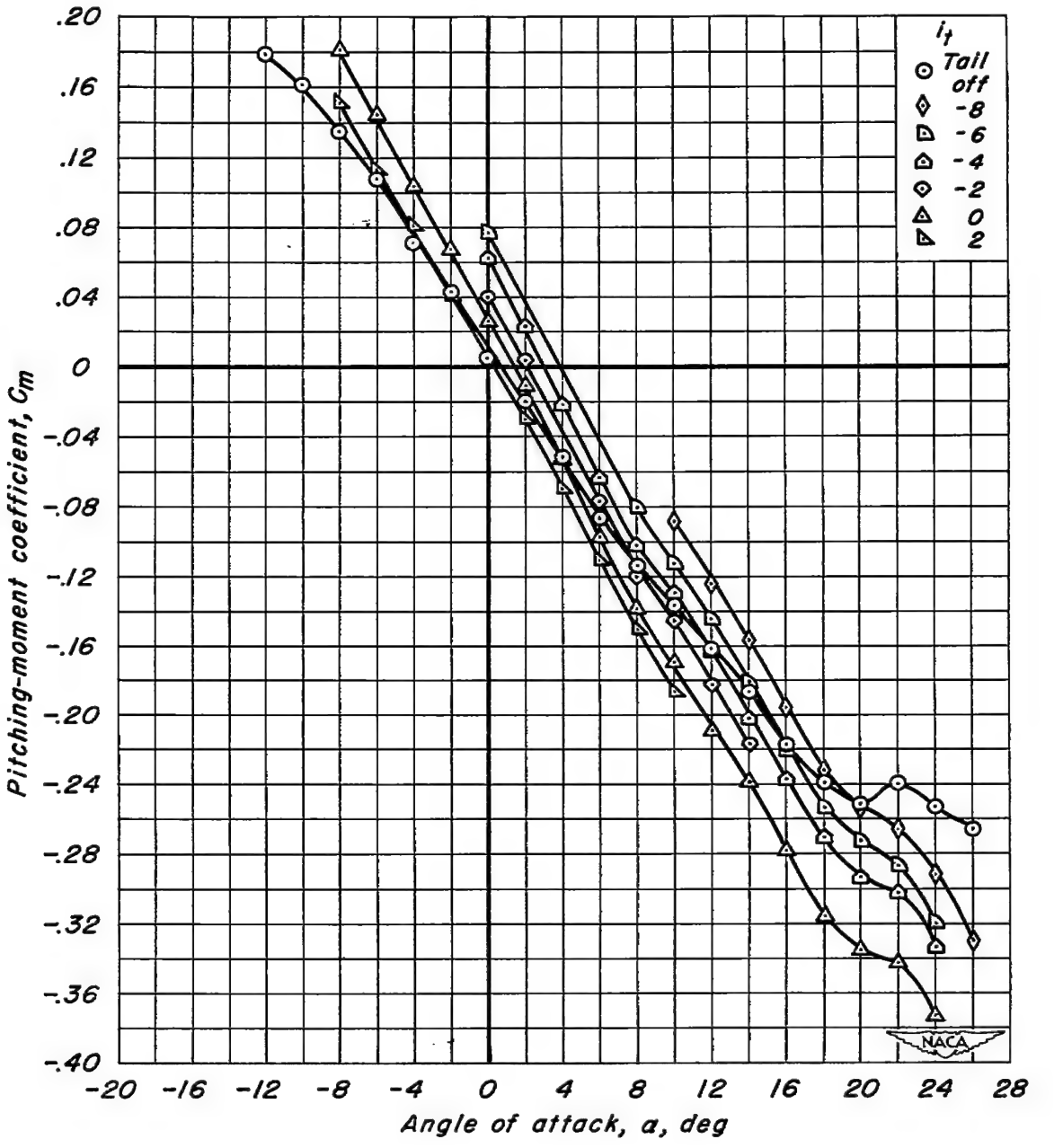

(c) M, 1.10

Figure 8.- Concluded.

[redacted]

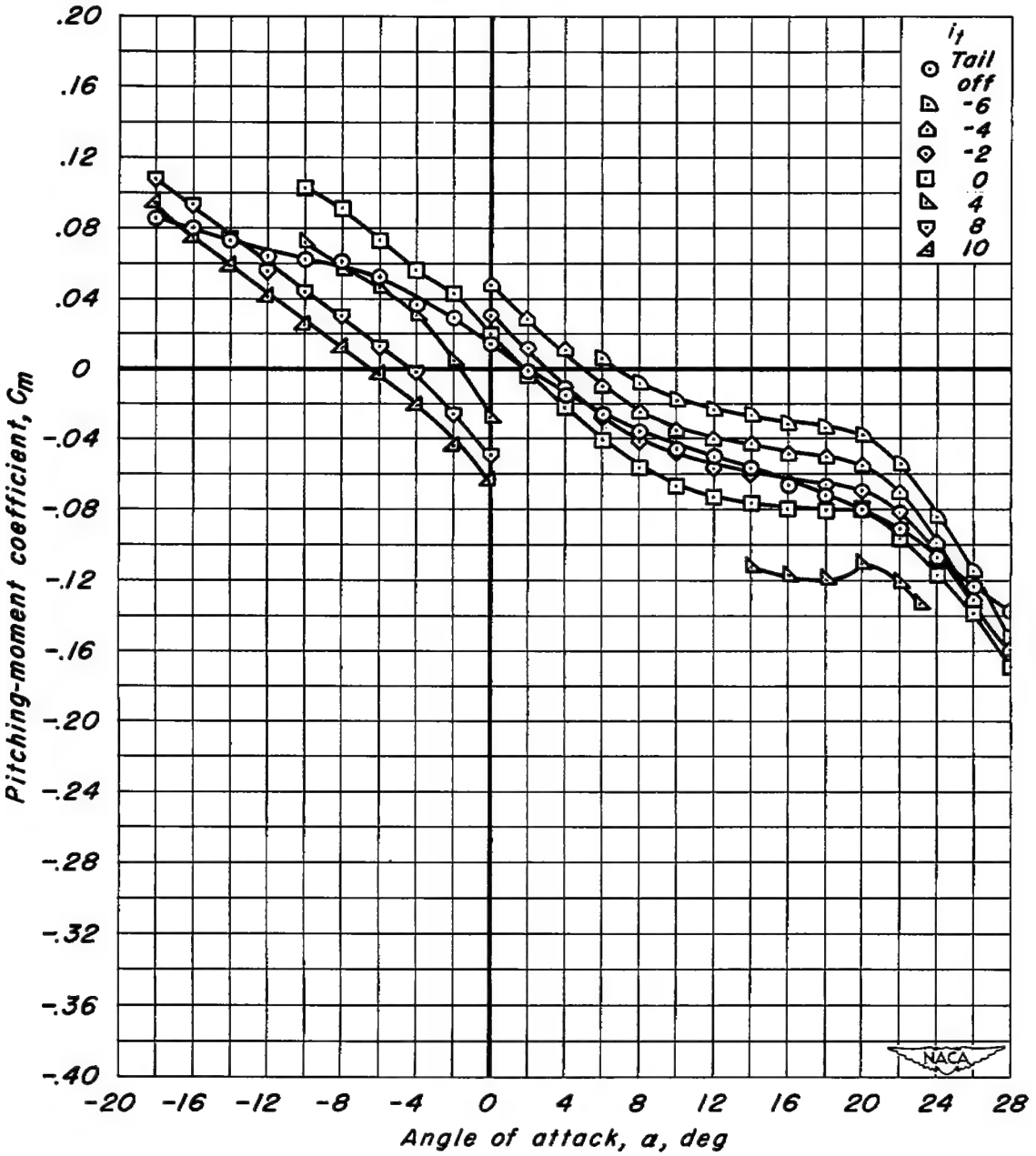

(a) M, 0.60

Figure 9.- Variation of pitching-moment coefficient with angle of attack for several incidence angles of the horizontal tail in position 2.

[redacted]

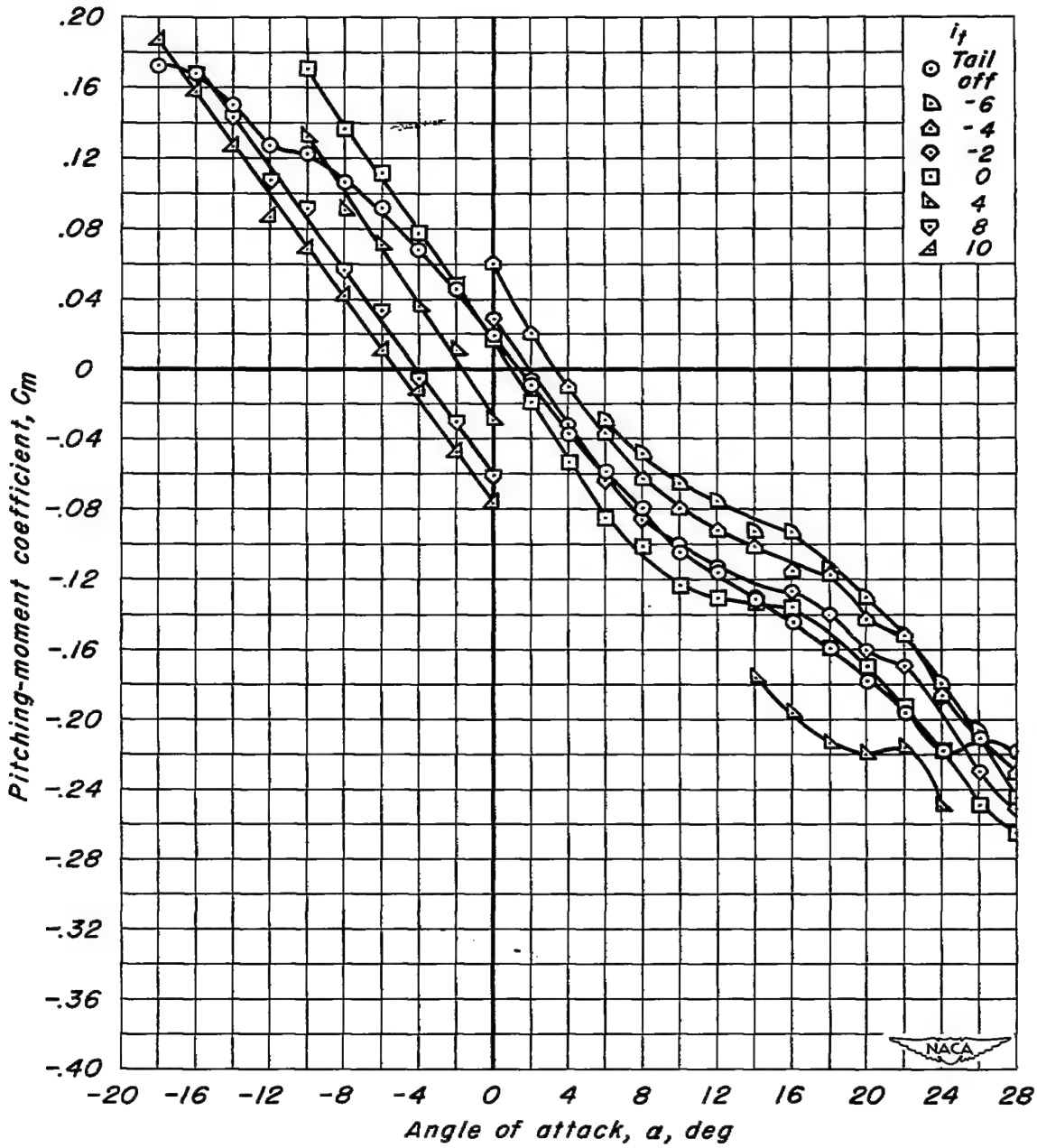

(b) M, 0.98

Figure 9.- Continued.

[redacted]

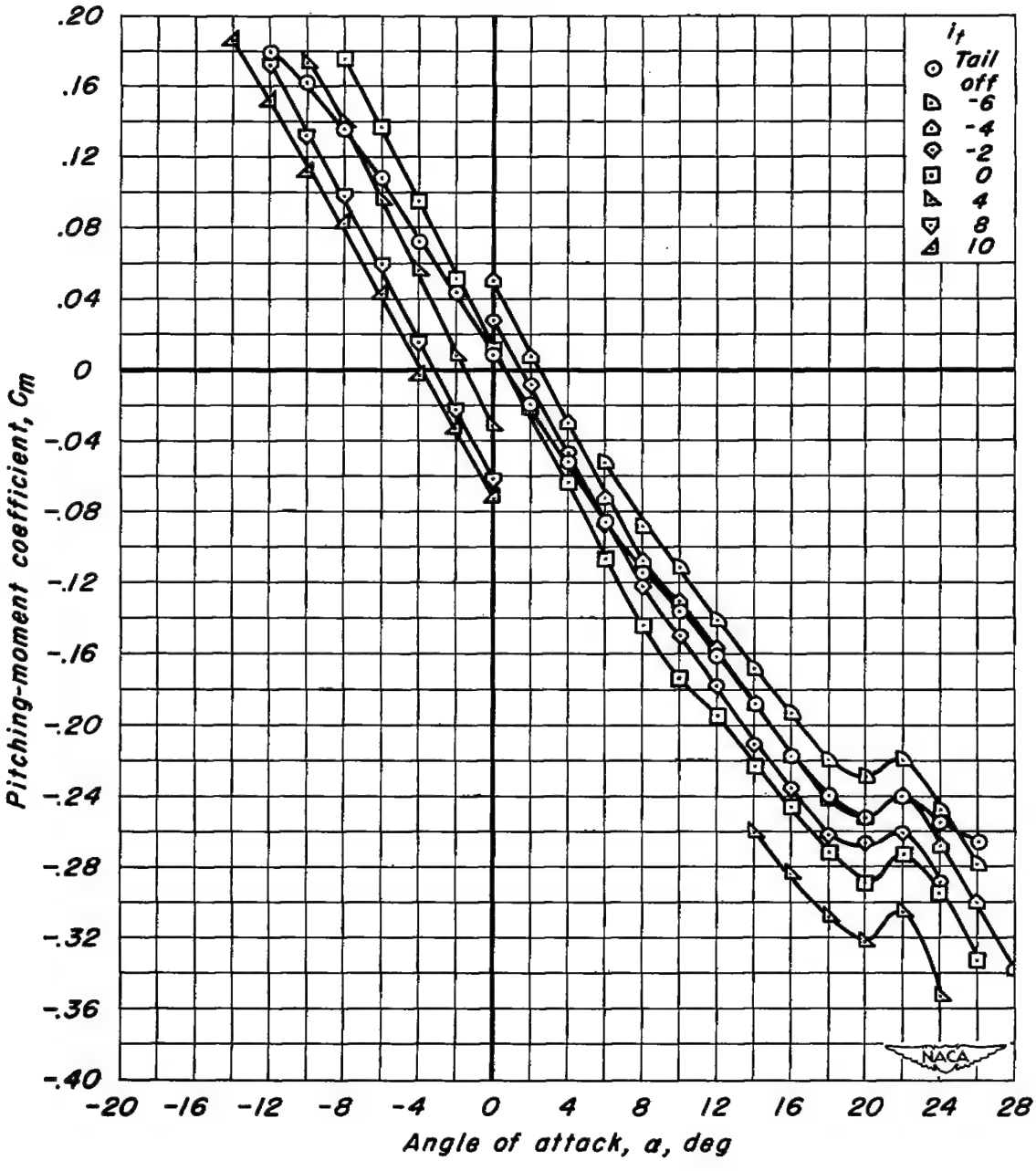

(c) M, 1.10

Figure 9.- Concluded.

[redacted]

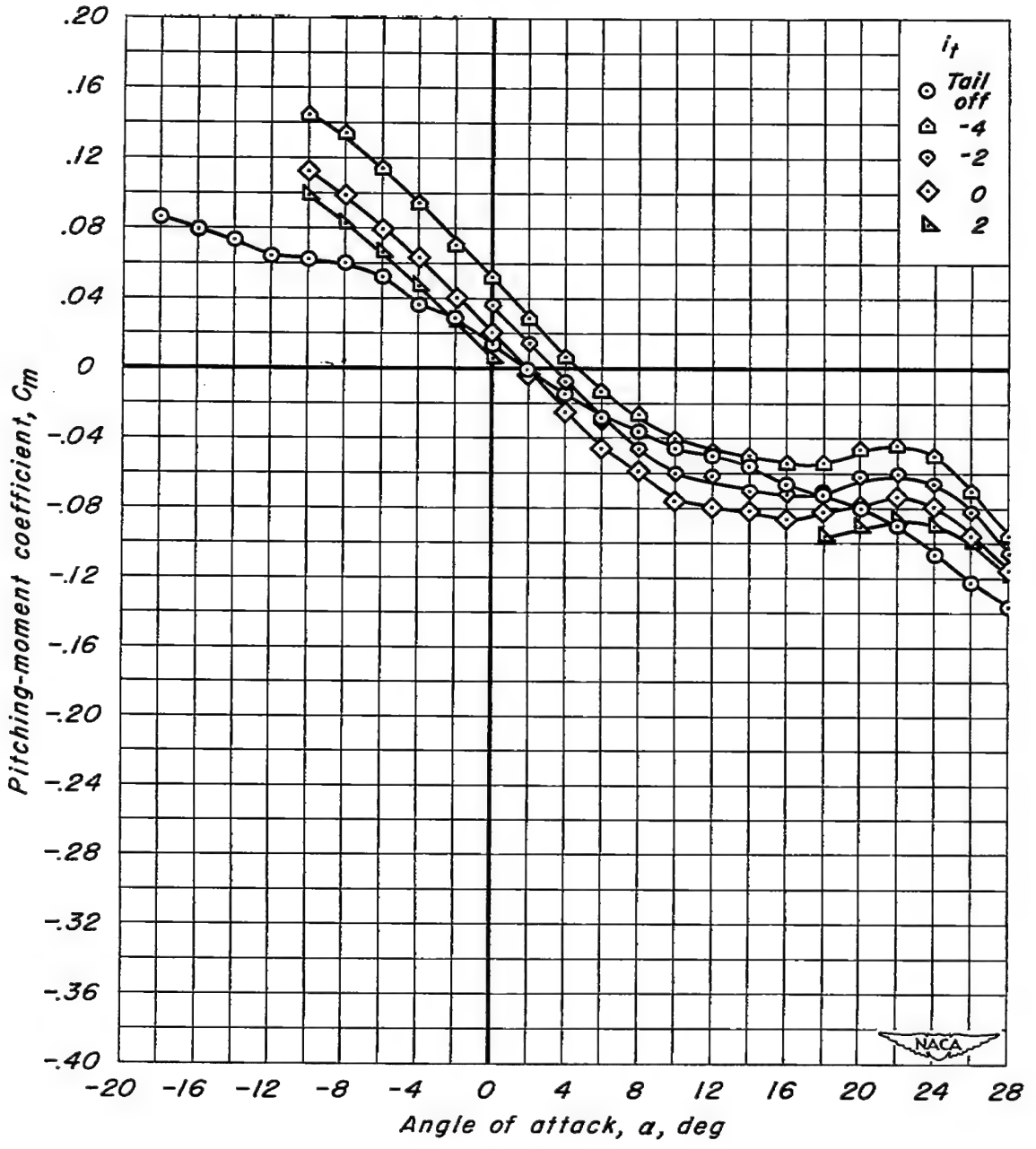

(a) M, 0.60

Figure 10.- Variation of pitching-moment coefficient with angle of attack for several incidence angles of the horizontal tail in position 3.

[redacted]

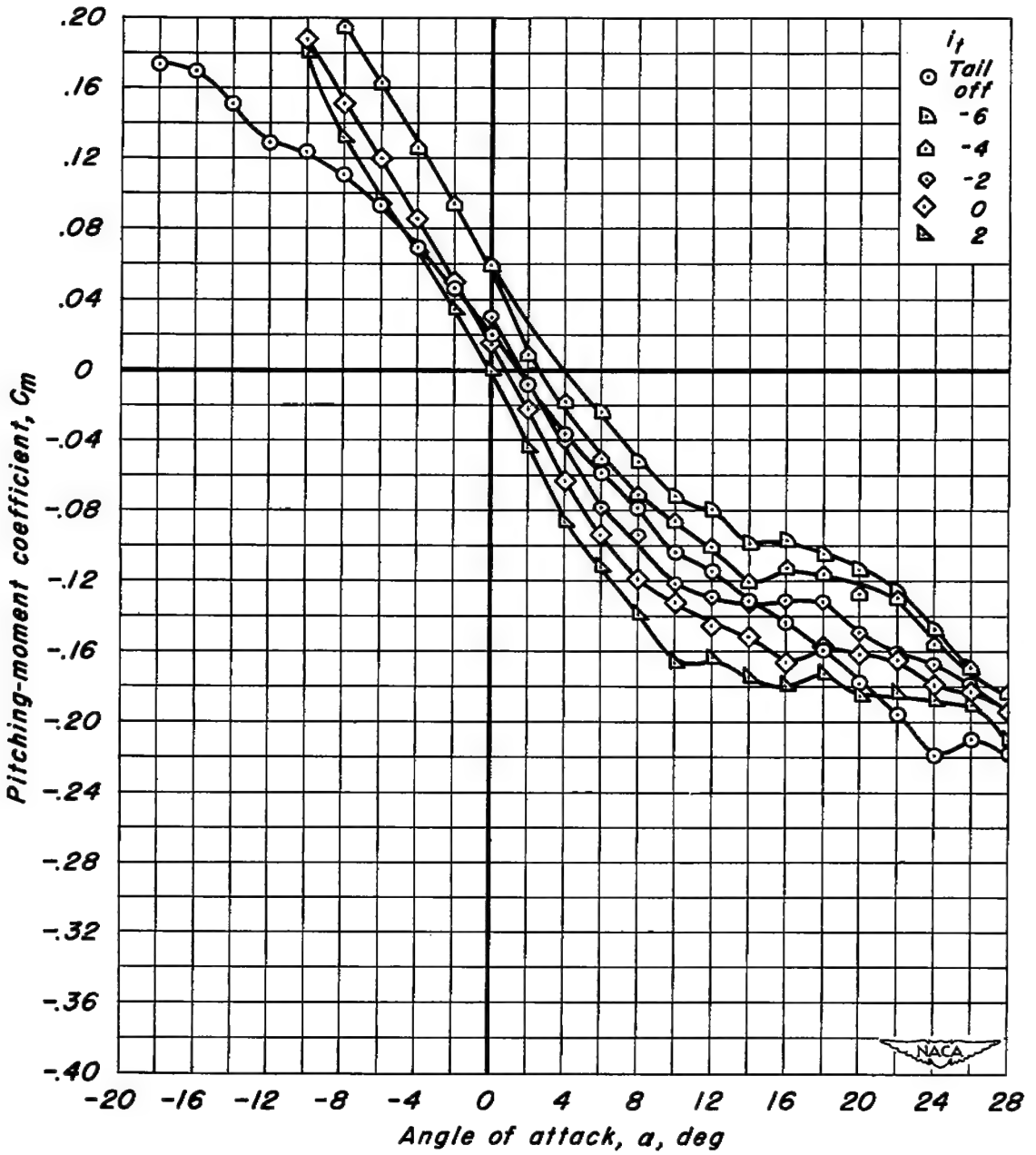

(b) M, 0.98

Figure 10.- Continued.

[redacted]

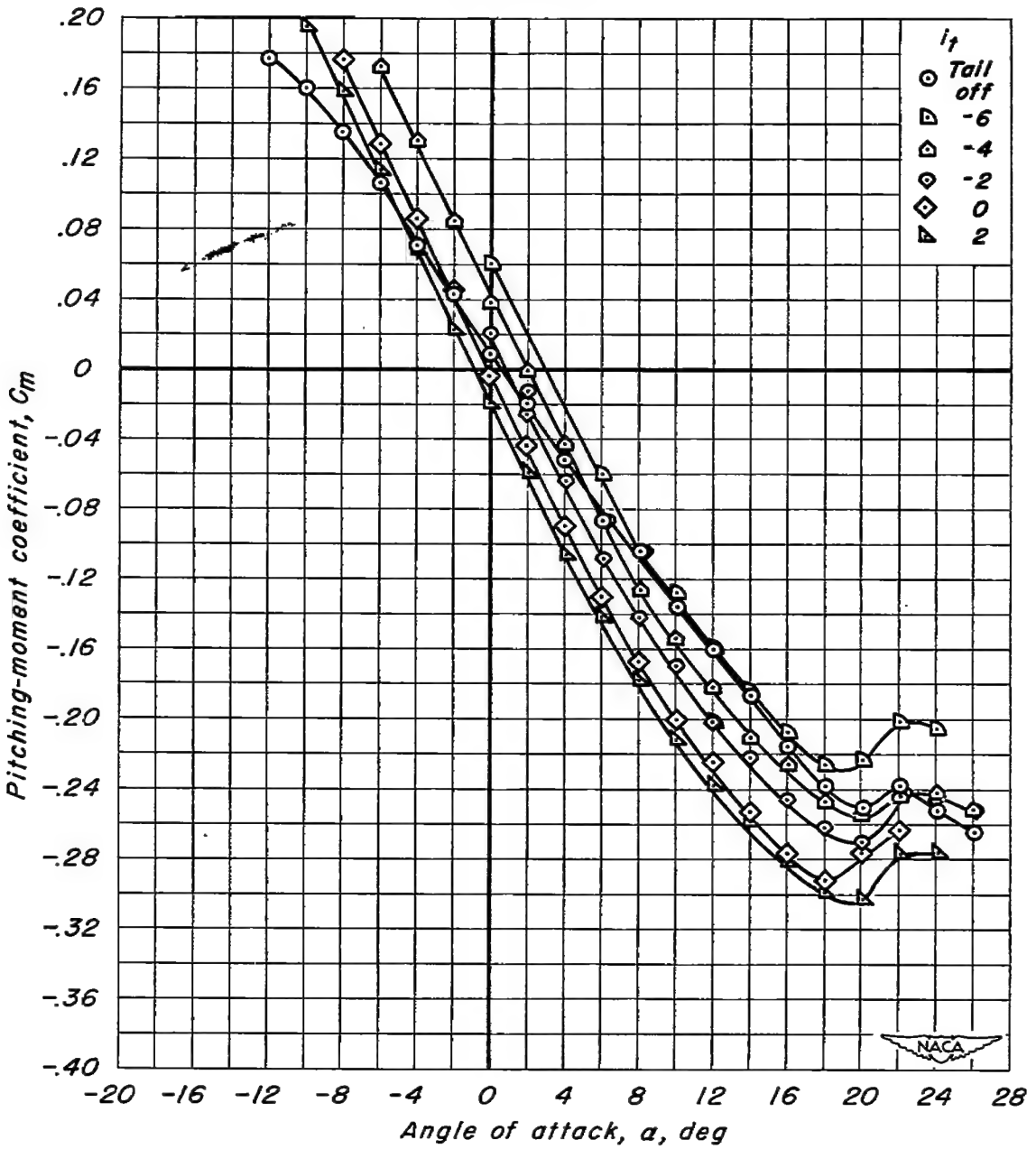

(c) M, 1.10

Figure 10.- Concluded.

[redacted]

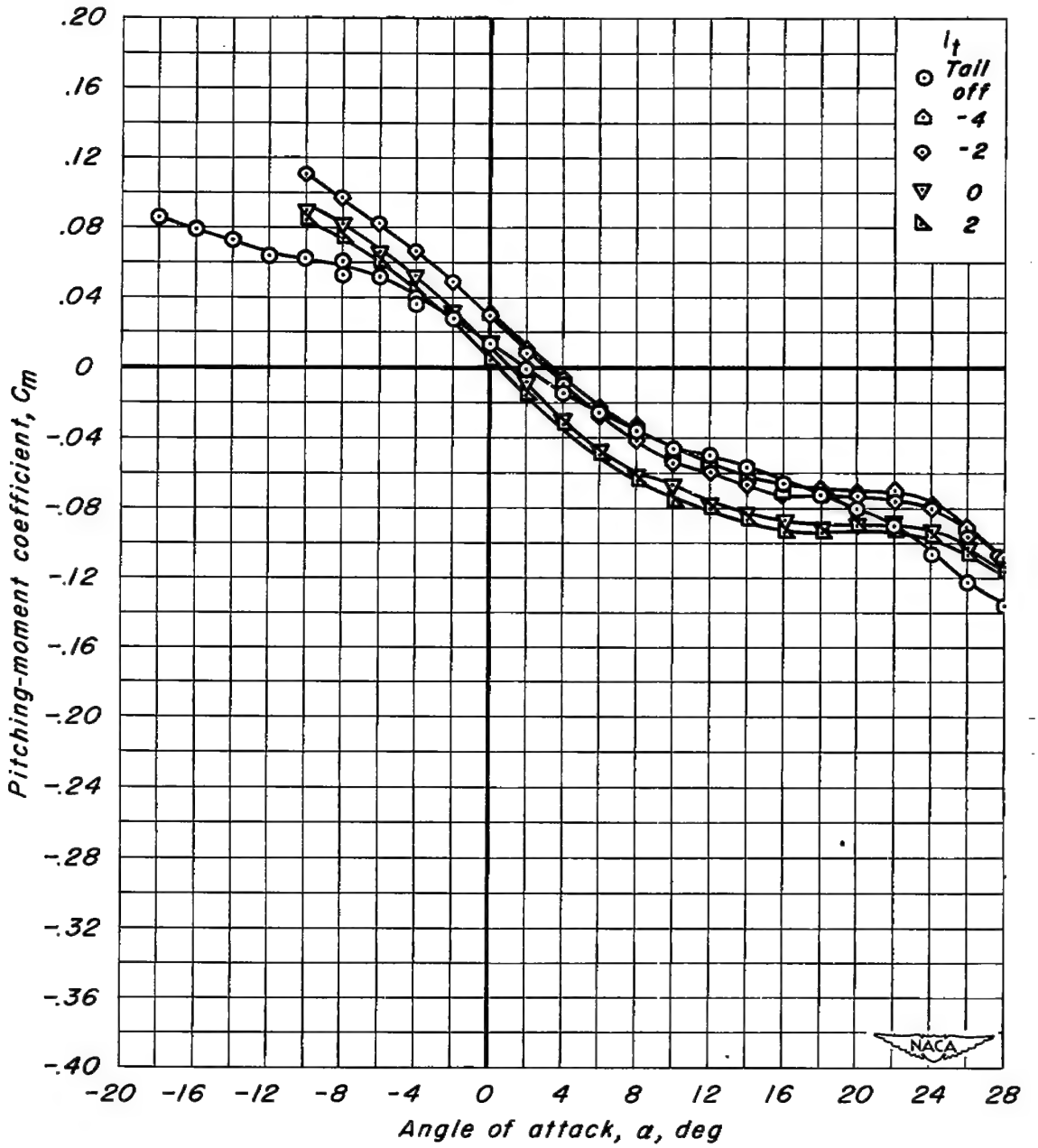

(a) M, 0.60

Figure 11.- Variation of pitching-moment coefficient with angle of attack for several incidence angles of the horizontal tail in position 4.

[redacted]

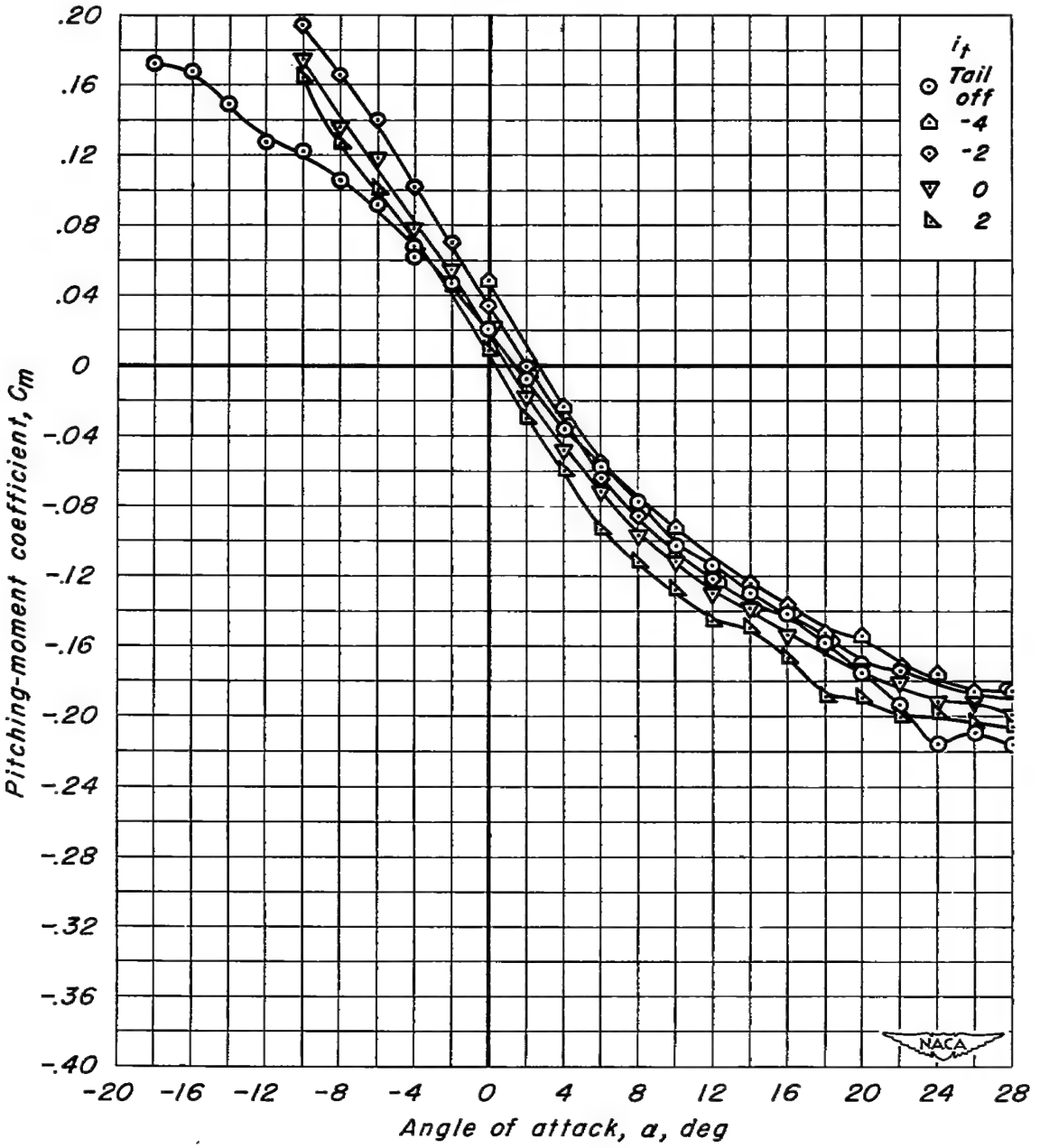

(b) M, 0.98

Figure 11.- Continued.

[redacted]

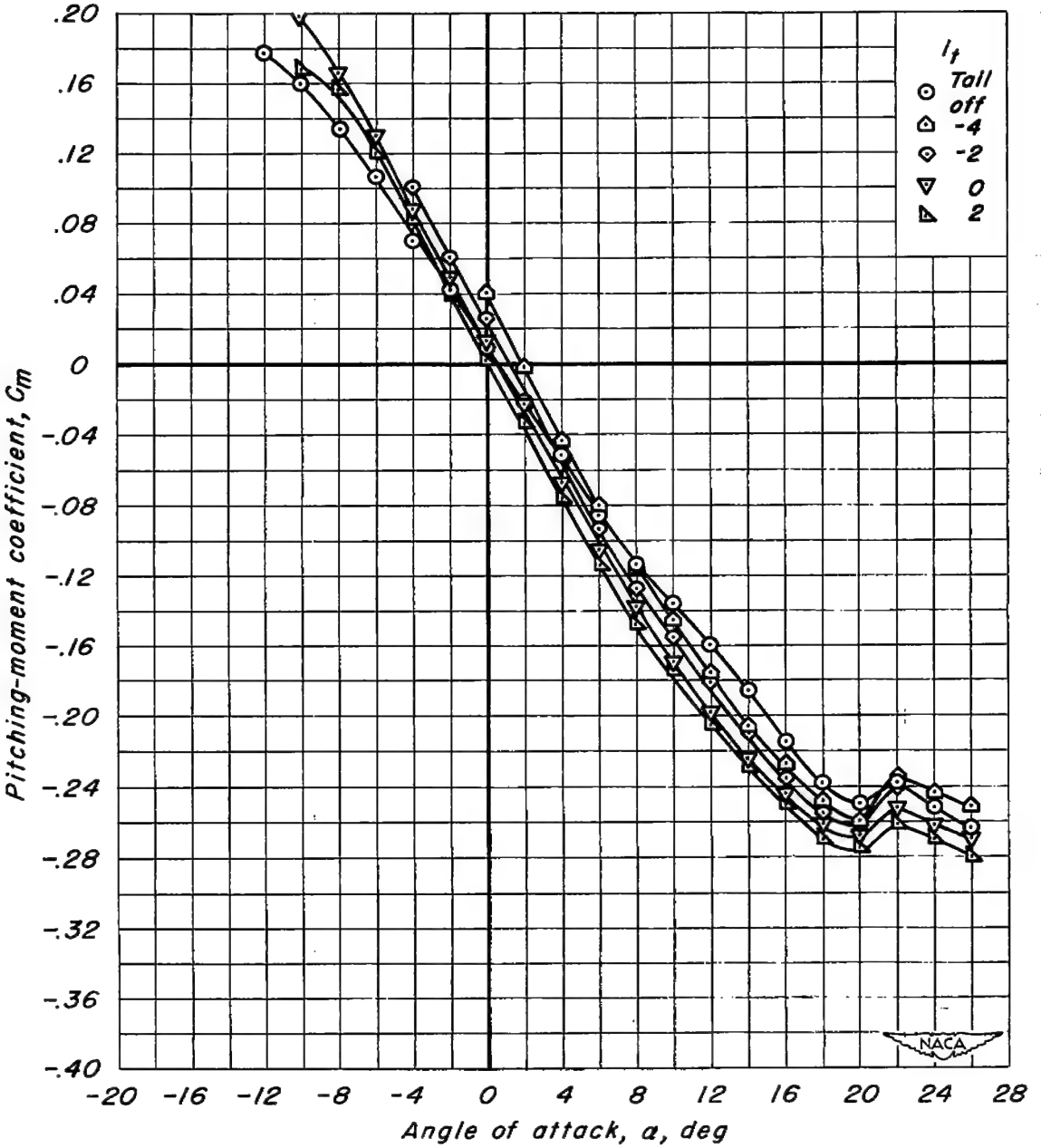

(c) M, 1.10

Figure 11.- Concluded.

[redacted]

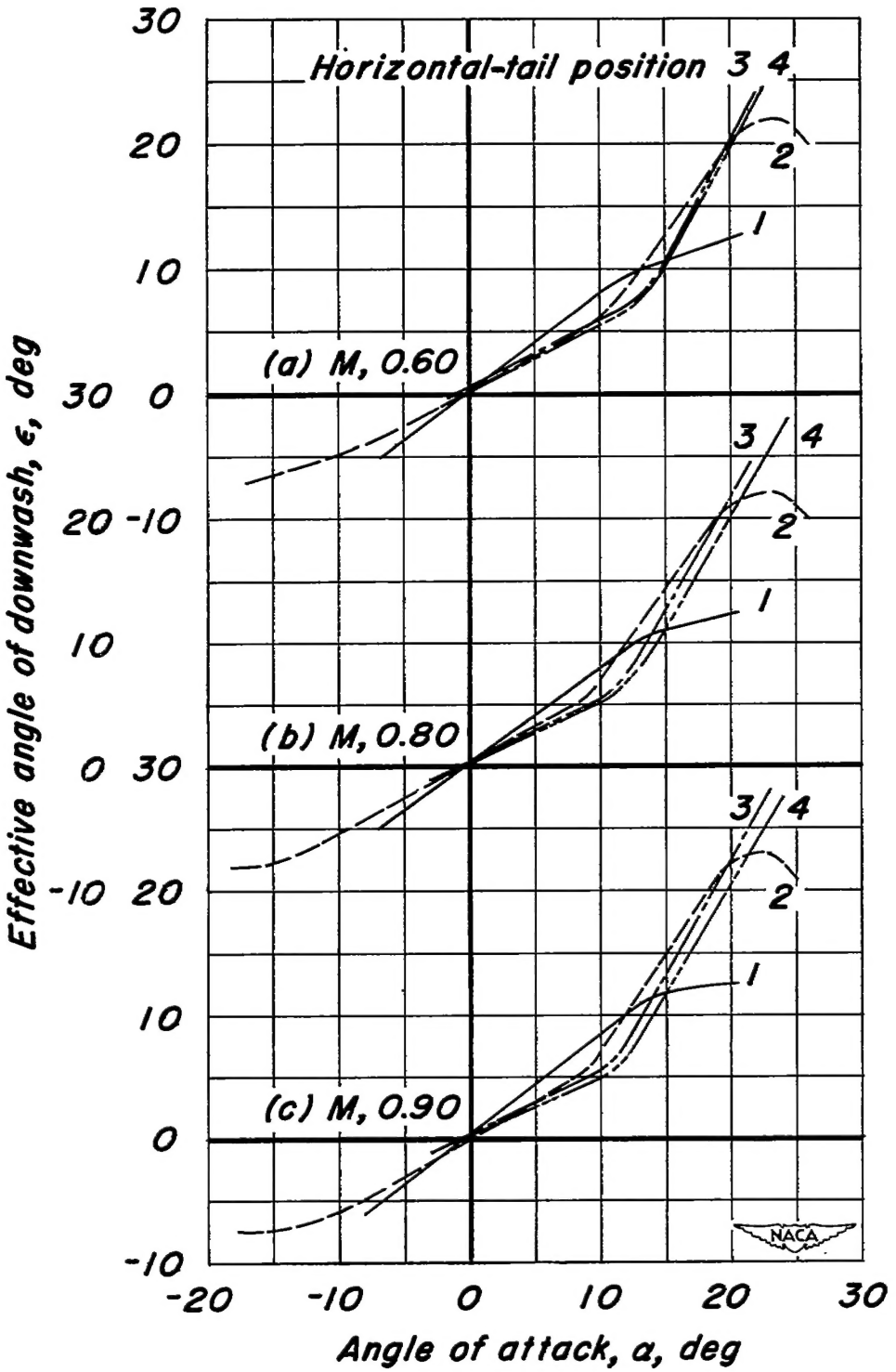

(a) Subsonic Mach numbers.

Figure 12.- Variation of effective downwash angle with angle of attack.

[redacted]

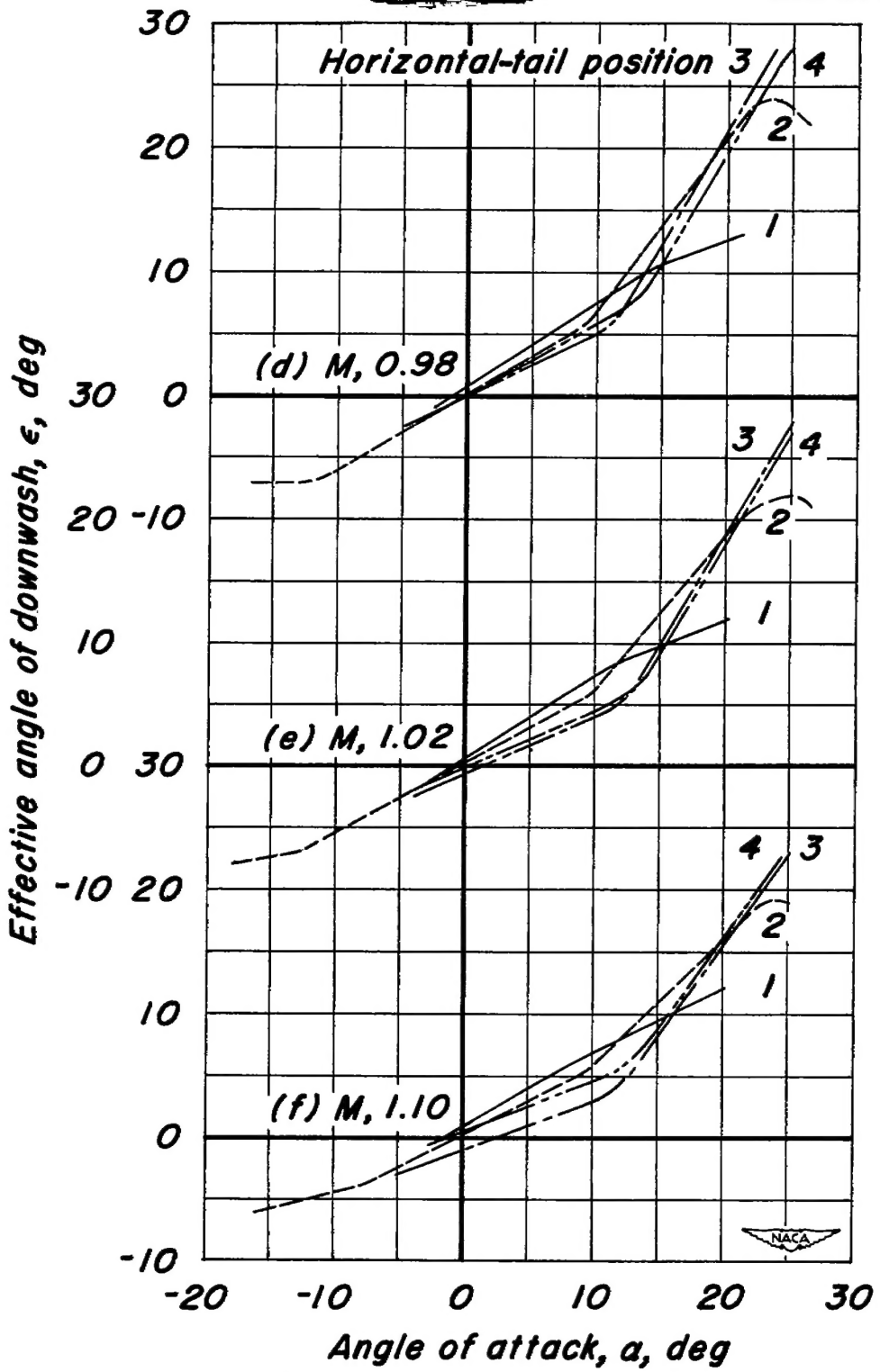

(b) Transonic Mach numbers.

Figure 12.- Concluded.

[redacted]

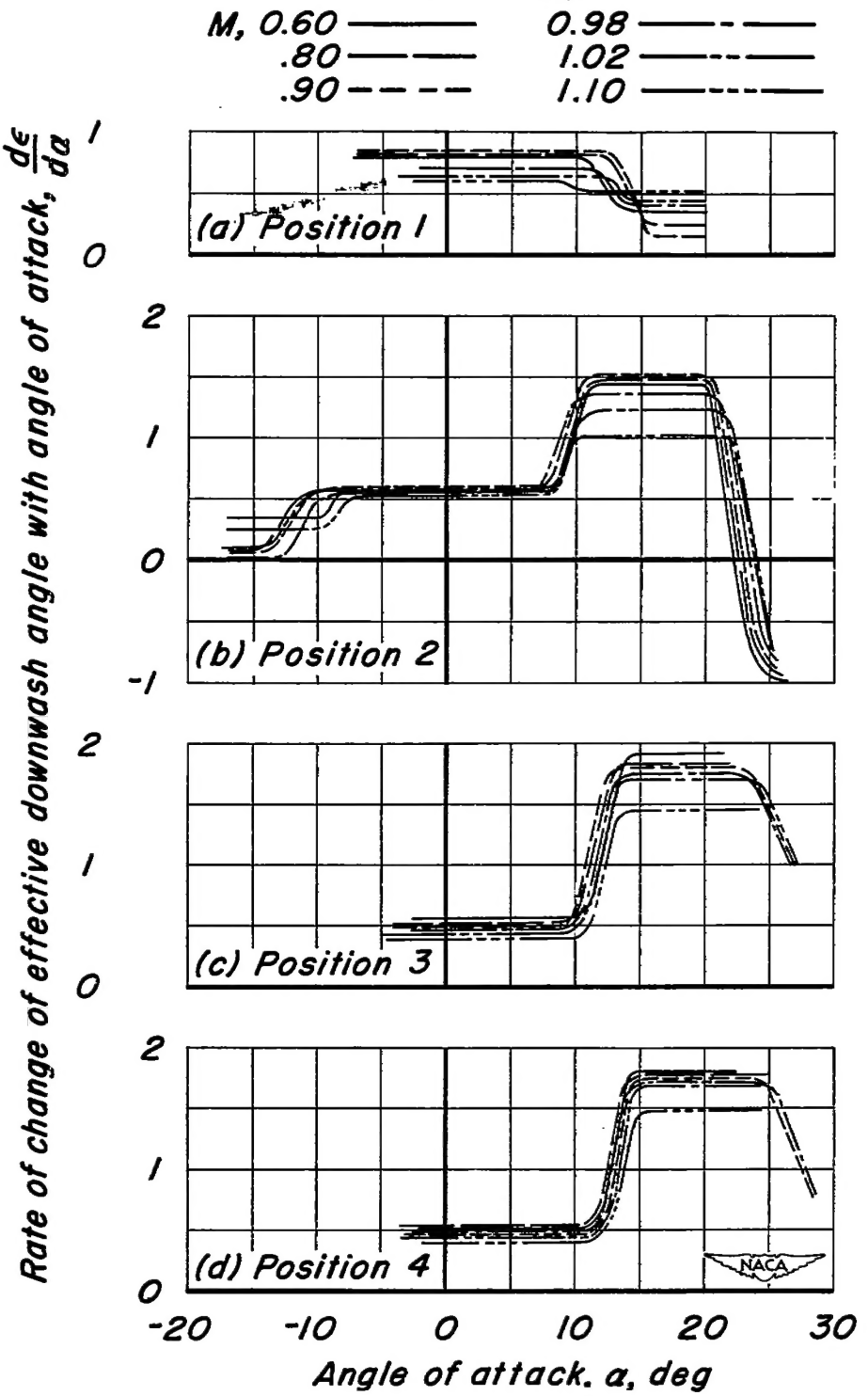

Figure 13.- Rate of change of effective downwash angle with angle of attack.

[redacted]

[redacted]

[redacted]